J. Fluid Mech. (2006), *vol.* 550, *pp.* 207–242. © 2006 Cambridge University Press
doi:10.1017/S0022112005008128 Printed in the United Kingdom

The energy cascade in a strongly stratified fluid

By ERIK LINDBORG

Department of Mechanics, KTH, S-100 44 Stockholm, Sweden
erikl@mech.kth.se

(Received 12 January 2005 and in revised form 19 August 2005)

A cascade hypothesis for a strongly stratified fluid is developed on the basis of the Boussinesq equations. According to this hypothesis, kinetic and potential energy are transferred from large to small scales in a highly anisotropic turbulent cascade. A relation for the ratio, l_v/l_h, between the vertical and horizontal length scale is derived, showing how this ratio decreases with increased stratification. Similarity expressions are formulated for the horizontal and vertical spectra of kinetic and potential energy. A series of box simulations of the Boussinesq equations are carried out and a good agreement between the proposed hypothesis and the simulations is seen. The simulations with strongest stratification give horizontal kinetic and potential energy spectra of the form $E_{K_h} = C_1\epsilon_K^{2/3}k_h^{-5/3}$ and $E_{P_h} = C_2\epsilon_P k_h^{-5/3}/\epsilon_K^{1/3}$, where k_h is the horizontal wavenumber, ϵ_K and ϵ_P are the dissipation of kinetic and potential energy, respectively, and C_1 and C_2 are two constants. Within the given numerical accuracy, it is found that these two constants have the same value: $C_1 \approx C_2 = 0.51 \pm 0.02$.

1. Introduction

The horizontal mesoscale (wave lengths ~1–500 km) wavenumber spectra of kinetic and potential energy measured in the upper troposphere and lower stratosphere (Vinnichenko 1970; Nastrom, Gage & Jasperson 1984; Nastrom & Gage 1985) have been debated for several decades. It is a remarkable feature of these spectra that they exhibit a $k_h^{-5/3}$-dependence, just as the spectrum of three-dimensional isotropic turbulence. This is seen in figure 1, where we have reproduced the classical spectra from Nastrom & Gage (1985). It has often been speculated (e.g. Gage 1979; Lilly 1983; Métais *et al.* 1996) that these spectra can be explained by the existence of an inverse cascade of energy, from small to large scales, just as in two-dimensional turbulence (Kraichnan 1970). The opposite hypothesis has also been advocated, that the spectra arise from a forward cascade of nonlinearly interacting gravity waves (Dewan 1979; 1997). Observational and theoretical work by Cho & Lindborg (2001), Lindborg & Cho (2000, 2001*a*) and Lindborg (2002) give support to the forward cascade hypothesis. There is also some evidence from numerical investigations supporting this hypothesis rather than the inverse cascade hypothesis. Koshyk & Hamilton (2001) have performed high-resolution general circulation model simulations exhibiting a quite realistic mesoscale spectrum. They conclude that 'the $-5/3$ spectral regime is not a quasi-2D inertial subrange', but 'contains a significant gravity wave component'. Riley & deBruynKops (2003) have performed high-resolution direct numerical simulations of strongly stratified freely decaying turbulence which clearly show a forward cascade type of dynamics with horizontal energy spectra exhibiting an inertial range very close to $k_h^{-5/3}$. Waite & Bartello (2004) have performed simulations of strongly stratified turbulence which is forced in large-scale vortical modes and

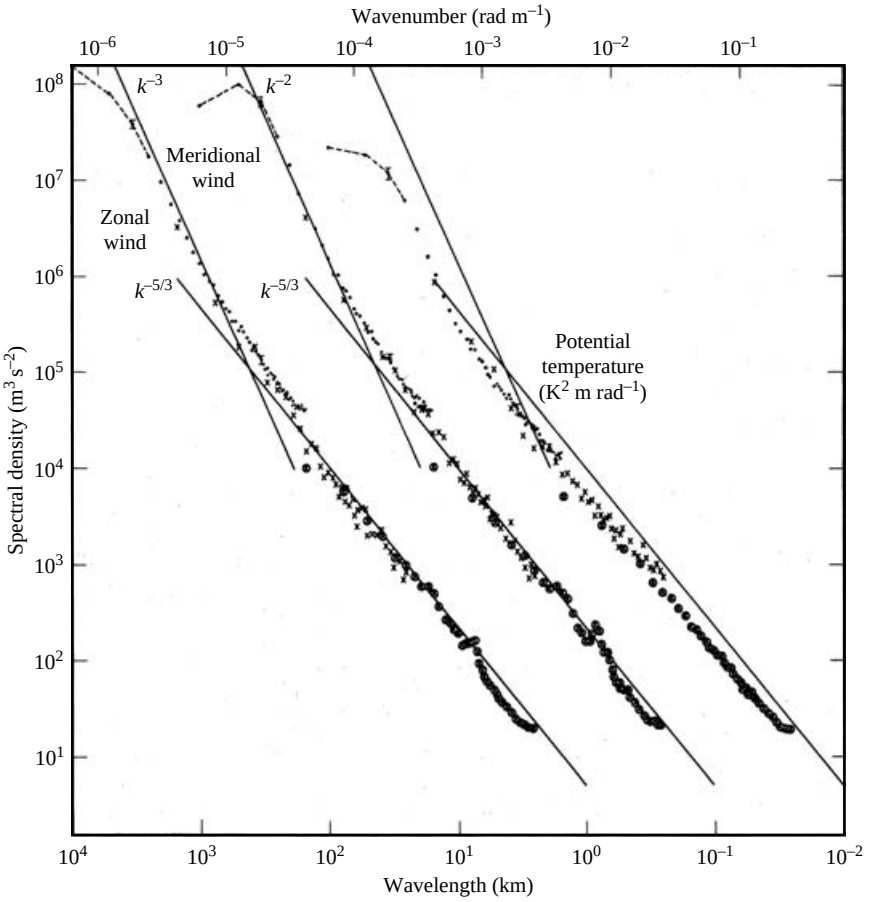

FIGURE 1. From left to right: variance power spectra of zonal wind, meridional wind and potential temperature near the tropopause from Global Atmospheric Sampling Program aircraft data. The spectra for meridional wind and temperature are shifted one and two decades to the right, respectively. [Reproduced from Nastrom & Gage 1985.]

which reaches a nearly stationary state, suggesting that there is a flux of energy from large to small scales. They see no signs of an inverse cascade. Skamarock (2004) has performed a large statistical study of high-resolution forecast simulations, initialized with large-scale fields corresponding to observed data. He found that the $k_h^{-5/3}$-range develops from initial fields lacking all mesoscale variability. The computed spectra show a remarkable similarity with the Nastrom–Gage spectrum. This clearly suggests that the energy of the mesoscale motions emanates from larger scales rather than smaller scales of motion.

In this paper, we develop the forward cascade hypothesis further and develop a similarity hypothesis for such a cascade. To do this, not only the horizontal energy spectra should be considered, but also the vertical energy spectra. Balloon measurements (Dewan & Good 1986; Cot 2001) show that vertical one-dimensional kinetic and potential energy spectra have a range of wavenumbers, corresponding to wave lengths $\sim$100–1000 m, with a k_v^{-3}-dependence, or very close to such a dependence. In figure 2, we have reproduced the vertical spectra measured by Cot (2001), using rising ballons. Such spectra are traditionally interpreted as originating from linear

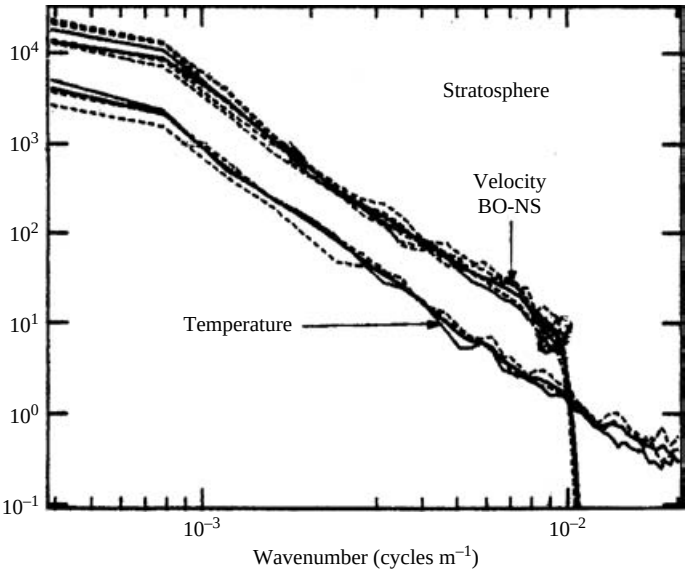

FIGURE 2. Vertical spectra of horizontal velocity and temperature from the statosphere. [Reproduced from Cot 2001.]

internal gravity waves. Here, we shall assume that they should instead be interpreted as arising from one and the same type of nonlinear chaotic motion as is giving rise to the horizontal $k_h^{-5/3}$-spectrum, and that this motion is governed by the fully nonlinear Boussinesq equations.

2. Hypothesis

The Boussinesq equations in a non-rotating frame of reference can be written

$$\frac{\partial \boldsymbol{u}}{\partial t} + (\boldsymbol{u}\cdot\nabla)\boldsymbol{u} = -\nabla p + \nu\Delta\boldsymbol{u} + N\boldsymbol{e}_z\phi, \tag{1}$$

$$\frac{\partial \phi}{\partial t} + (\boldsymbol{u}\cdot\nabla)\phi = \kappa\Delta\phi - Nw, \tag{2}$$

$$\nabla\cdot\boldsymbol{u} = 0. \tag{3}$$

Here, $\boldsymbol{u}$ is the velocity field, ν and κ are, respectively, the kinematic molecular viscosity and diffusivity, $\boldsymbol{e}_z$ is the vertical unit vector, N is the Brunt–Väisälä frequency, $\phi = gT'/(NT_o)$, where T' and T_o are the fluctuating and equilibrium temperatures, respectively, g is the acceleration due to gravity and $w = \boldsymbol{e}_z\cdot\boldsymbol{u}$ is the vertical velocity component.

In this paper, we will not consider the case with system rotation although Coriolis effects are generally very important in the atmosphere. The $k_h^{-5/3}$-range seen in figure 1, continues up to fairly large wavenumbers corresponding to wave lengths of about 1 km. At these scales, Coriolis effects are by all likelihood of minor importance. If there is a single physical mechanism behind the generation of the whole $k_h^{-5/3}$-range, which is very plausible, it is therefore reasonable to seek this mechanism without introducing Coriolis effects at first. In this respect, we differ from Tung & Orlando (2003) who claim to have reproduced the whole spectrum range seen in figure 1, including both the k_h^{-3}-range and the $k_h^{-5/3}$-range, in a quasi-geostrophic (rotationally

dominated) two-level model simulation. For the k_h^{-3}-range, the claim seems to be justified. However, as for the $k_h^{-5/3}$-range which is produced for the very highest wavenumbers, it remains to be shown that this is not an artefact of too low a resolution, as pointed out by Smith (2004). In a companion paper (Lindborg 2005), we present a series of numerical simulations including system rotation and show that the results presented in this paper also are valid in the case with system rotation, provided that this is not too strong.

Apart from total energy, the inviscid Boussinesq equations conserve potential vorticity, $\Pi = \nabla \times \boldsymbol{u} \cdot (\nabla\phi + \boldsymbol{e}_z N)$. The theoretical argument that is often developed in favour of the inverse cascade hypothesis is that the existence of a second conserved quantity should lead to an inverse energy cascade just as in two-dimensional turbulence, where the second conserved quantity is enstrophy. This argument can be valid if it can be shown that $\nabla \times \boldsymbol{u} \cdot \nabla\phi \ll \nabla \times \boldsymbol{u} \cdot \boldsymbol{e}_z N$ in the strongly stratified limit, so that $\Pi \approx \nabla \times \boldsymbol{u} \cdot \boldsymbol{e}_z N$. If this were the case, the vertical component of vorticity would be approximately conserved at a fluid particle, and the dynamics would be very much like two-dimensional turbulence or quasi-geostrophic turbulence. In the latter case, conservation of potential vorticity can actually lead to an inverse energy cascade, as shown by Charney (1971). In the general case, however, this is not so. This can be seen by considering the limit of no stratification, that is when $N = 0$. In this limit, the system (1)–(3) reduces to the traditional incompressible Navier–Stokes equations together with the equation for the scalar ϕ, which in this case is a purely passive scalar. Potential vorticity is still conserved and is generally not equal to zero. The solutions of the equations includes classical three-dimensional Kolmogorov turbulence with a forward energy cascade as well as a forward cascade of scalar concentration $\phi\phi/2$. According to the scaling hypothesis developed in this paper and also developed by Billant & Chomaz (2001), the term $\nabla \times \boldsymbol{u} \cdot \nabla\phi$ will be at least of the same order as the term $\nabla \times \boldsymbol{u} \cdot \boldsymbol{e}_z N$ in the limit of strong stratification. Hence, if this scaling hypothesis is correct, there is no reason to believe that the energy cascade should be in the inverse direction for strongly stratified flows. It seems more reasonable to believe that it should be in the forward direction.

To make it plausible that the vertical k_v^{-3}-spectra starting at wavenumbers corresponding to the length scale $l_v \sim 1\,\mathrm{km}$, arise from the same forward cascade dynamics as the horizontal $k_h^{-5/3}$-spectrum, starting at wavenumbers corresponding to the length scale $l_h \sim 500\,\mathrm{km}$, we must derive a relation for the length scale ratio l_v/l_h. To do this, we consider a system, governed by (1)–(3), in which kinetic energy is injected at a rate P, in the form of large vertically oriented vortices with horizontal length scale l_h. In the absence of vertical shear, this system should, according to conventional wisdom, be very stable. However, we assume that the system will become unstable very much in the same way as a system undergoing the 'zigzag instability' discovered by Billant & Chomaz (2000*a*, *b*) or the 'tall-column instability' investigated by Dritschel & de la Torre Juárez (1996). These instabilities set in if the stratification is strong enough and introduce strong vertical gradients into a system which is originally lacking any vertical variation. We further assume that a chaotic state will develop subsequently in which energy cascades from large scales of motion to small scales of motion. For a statistically stationary and homogeneous system the equations for mean kinetic and potential energy, $E_K = \frac{1}{2}\langle \boldsymbol{u} \cdot \boldsymbol{u} \rangle$ and $E_P = \frac{1}{2}\langle \phi\phi \rangle$, can be derived from (1)–(3)

$$0 = P - \epsilon_K + N\langle \phi w \rangle, \tag{4}$$

$$0 = -\epsilon_P - N\langle \phi w \rangle, \tag{5}$$

where ϵ_K and ϵ_P are the dissipation of kinetic and potential energy, respectively. The potential energy content in the $k_h^{-5/3}$-range of the spectrum in figure 1 and in the k_v^{-3}-range of the spectrum in figure 2, is of the same order of magnitude as the corresponding kinetic energy content. Billant & Chomaz (2001) have shown that there is a fundamental scale invariance in the Boussinesq equations in the limit of strong stratification, and that this invariance implies an approximate equipartition of energy between kinetic and potential energy. We will instead, as a starting point, assume that there is approximate equipartion in the fully developed system, and show that the Billant & Chomaz invariance follows as a consequence of this assumption. Thus, we assume that $E_P \sim E_K, \quad \phi \sim u$ and $\epsilon_P \sim \epsilon_K$, where u is a horizontal velocity component. We also adopt the classical estimates by Taylor (1935),

$$u \sim (l_h \epsilon)^{1/3}, \quad E_K \sim (l_h \epsilon)^{2/3}. \tag{6}$$

where $\epsilon = \epsilon_K + \epsilon_P$. The continuity equation (3) gives $w \sim l_v u / l_h$. By applying these estimates to the energy equations (4)–(5) we find

$$\frac{l_v}{l_h} \sim \frac{\epsilon^{1/3}}{N l_h^{2/3}} \equiv F_h, \tag{7}$$

where the Froude number F_h is an inverse measure of the strength of the stratification. From (4)–(5) it follows that $P = \epsilon$ and F_h is therefore determined by the three parameters N, P and l_h which are imposed on the system. From (7), directly follows the relation

$$\frac{l_v}{l_O} \sim F_h^{-1/2}, \tag{8}$$

where $l_O = \epsilon^{1/2}/N^{3/2}$ is the Ozmidov length scale, which is about the smallest scale for which the strongly stratified cascade hypothesis can be applied. Thus, (8) is an estimate of the range of vertical scales for which the hypothesis is supposed to be valid.

Implicit in the assumption of the existence of a cascade is the assumption that nonlinear inertial forces cannot be neglected, since it is only through such forces that a cascade can be maintained. The ratio between inertial forces and buoyancy forces can be measured by the vertical Froude number $F_v = u/(N l_v)$. It is easily verified that (6) and (7) also give

$$F_v \sim 1, \tag{9}$$

which is the basic invariance implied by the analysis of Billant & Chomaz (2001). Indeed, the result (7) can also be directly derived by combining (9) with Taylor's estimate (6). The hypothesis presented in this paper, can thus be interpreted as stating that, in the limit of low F_h, the statistically stationary solutions of the Boussinesq equations are characterized by a forward energy cascade which is not violating the Billant & Chomaz invariance. That $F_v \sim 1$ means that inertial forces will be of the same order as buoyancy forces, no matter how strong the stratification is. For a given horizontal length scale l_h, the vertical length scale will adjust so as to maintain the balance between inertia and buoyancy. When the stratification is stronger the vertical gradients will become stronger and the vertical length scale will become smaller.

For low Froude numbers, there will be a strong separation between the vertical and horizontal length scales, i.e. $l_v \ll l_h$. In such a case, it is reasonable to assume that only the horizontal length scale enters into the expressions for the horizontal energy spectra and only the vertical length scale enters into the expressions for the vertical spectra. We therefore assume that the horizontal one-dimensional energy spectra of

kinetic and potential energy are of the similarity form

$$E_{K_h}(k_h) = u^2 l_h \tilde{E}_{K_h}(k_h l_h) \sim \epsilon^{2/3} l_h^{5/3} \tilde{E}_{K_h}(k_h l_h), \tag{10}$$

$$E_{P_h}(k_h) = u^2 l_h \tilde{E}_{P_h}(k_h l_h) \sim \epsilon^{2/3} l_h^{5/3} \tilde{E}_{P_h}(k_h l_h), \tag{11}$$

and the corresponding vertical spectra are of the form

$$E_{K_v}(k_v) = u^2 l_v \tilde{E}_{K_v}(k_v l_v) \sim N^2 l_v^3 \tilde{E}_{K_v}(k_v l_v), \tag{12}$$

$$E_{P_v}(k_v) = u^2 l_v \tilde{E}_{P_v}(k_v l_v) \sim N^2 l_v^3 \tilde{E}_{P_v}(k_v l_v), \tag{13}$$

where the four functions with a tilde are dimensionless. Here, $k_v = |k_z|$ and k_h is the magnitude of the horizontal wavenumber corresponding to the direction in which the spectrum is measured. If, for example, the spectrum is measured in the x-direction, then $k_h = |k_x|$. The first forms written down in (10)–(13) of these similarity assumptions are, in fact, very weak. Assuming that each spectral quantity is determined by a single length scale l_h or l_v and the velocity scale u, they are the only possible similarity expressions. In the second form, Taylor's estimate (6) and the scale relation (7) have been used, which leads to very different scaling behaviour for the vertical and the horizontal spectra.

The maximum vertical wavenumber $k_{v_{max}}$ for which the similarity expressions (10)–(13) can hold will scale with the Ozmidov length scale, so that $k_{v_{max}} \sim 1/l_O$. At wavenumbers larger than $k_{v_{max}}$, the effect of stratification will not be strong enough to maintain this type of scaling and there will be a transition to classical three-dimensional turbulence. The corresponding maximum horizontal wavenumber $k_{h_{max}}$ will also scale with the Ozmidov length scale. However, $k_{h_{max}}$ will be considerably smaller than $k_{v_{max}}$.

For horizontal wavenumbers such that $1/l_h \ll k_h < k_{h_{max}}$, it can be assumed that the horizontal energy spectra should become independent of l_h, and for such wavenumbers we should therefore have

$$E_{K_h}(k_h) \sim E_{P_h}(k_h) \sim \epsilon^{2/3} k_h^{-5/3}. \tag{14}$$

Analogously, for vertical wavenumbers such that $1/l_v \ll k_v < k_{v_{max}}$, it can be assumed that the vertical energy spectra should become independent of l_v, and for such wavenumbers we should therefore have

$$E_{K_v}(k_v) \sim E_{P_v}(k_v) \sim N^2 k_v^{-3}. \tag{15}$$

These relations were suggested by Dewan (1997) based on similar assumptions to those made here. The vertical spectra (15) were also suggested by Billant & Chomaz (2001), as a direct consequence of their scaling theory. Lumley (1964) suggested a turbulence model spectrum exhibiting a transition from a k^{-3}-dependence in the low wavenumber end dominated by the effect of buoyancy to a $k^{-5/3}$-dependence in the high wavenumber end dominated by classical Kolmogorov turbulence. However, Lumley's model spectrum is isotropic as is the $k^{-11/5}$ spectrum for buoyancy-dominated turbulence suggested by Bolgiano (1959). Since these early works, numerous observations have shown that the strongest effect of buoyancy is to introduce different scaling behaviour in the vertical direction as compared to the horizontal direction rather than altering the shape of an isotropic spectrum.

To be able to test relation (7), we require an independent definition of the vertical length scale l_v. Assume that the vertical spectrum of kinetic energy scales as (12). Then, to within a constant factor of the order of unity, l_v can be determined from the

expression

$$\frac{\int_0^{k_{v_{max}}} E_{K_v}(k_v)\,\mathrm{d}k_v}{\int_0^{k_{v_{max}}} k_v E_{K_v}(k_v)\,\mathrm{d}k_v}, \tag{16}$$

Here, we will use this expression as the definition of l_v. We also define a corresponding length scale, l_v', over which the potential energy varies, as

$$l_v' = \frac{\int_0^{k_{v_{max}}} E_{P_v}(k_v)\,\mathrm{d}k_v}{\int_0^{k_{v_{max}}} k_v E_{P_v}(k_v)\,\mathrm{d}k_v}. \tag{17}$$

If the spectra fall off faster than k_v^{-2} as $k_v \to \infty$ then the upper integration limit $k_{v_{max}}$ in (16) and (17) can be replaced with ∞.

2.1. *Order of magnitude estimates*

Using realistic parameter values, we make order of magnitude estimates to check that the hypothesis that we have developed is realistic and also estimate the critical Froude number, $F_{h_{crit}}$, under which limit the hypothesis can be applied. We choose $l_h = 500\,\mathrm{km}$, $l_v = 1\,\mathrm{km}$, $N = 2 \times 10^{-2}\,\mathrm{s}^{-1}$ and $T_o = 225\,\mathrm{K}$. As for the value of ϵ, Cho & Lindborg (2001) and Lindborg & Cho (2001*b*) made the estimates $\epsilon_K = 6.0 \times 10^{-5}\,\mathrm{m^2\,s^{-3}}$ and $\epsilon_P = 2.0 \times 10^{-5}\,\mathrm{m^2\,s^{-3}}$, based on third-order structure-function calculations using airplane data from the lower stratosphere. Using the value $\epsilon = 8.0 \times 10^{-5}\,\mathrm{m^2\,s^{-3}}$, we find

$$F_h = 3.4 \times 10^{-4} \approx 0.2 l_v / l_h, \tag{18}$$

which we think is close enough to the estimate (7). For the typical velocity and temperature fluctuations, we find

$$u \sim (\epsilon l_h)^{1/3} \approx 3\,\mathrm{m\,s^{-1}}, \quad T' = T_o \phi N/g \sim T_o (\epsilon l_h)^{1/3} N/g \sim 1\,\mathrm{K}, \tag{19}$$

and for the eddy turnover time,

$$\tau = l_h^{2/3}/\epsilon^{1/3} \sim 40\,\mathrm{h}, \tag{20}$$

which all seem reasonable. As for the estimate of the critical Froude number, it has been observed (see figure 3 in Vinnichenko 1970) that there is a region in the horizontal energy spectra around a wavenumber corresponding to a wave length of 1 km, where the $k_h^{-5/3}$-range ends. Some of the measured spectra exhibit a sudden increase and some of the spectra exhibit a sudden decrease in magnitude for wavenumbers higher than this. We interpret these observations as evidence of a transition from the low-Froude-number asymptotic cascade, or 'stratified cascade motion' to classical three-dimensional turbulence. The critical Froude number can be estimated by setting $l_h = 1\,\mathrm{km}$. We thus find

$$F_{h_{crit}} \approx 0.02. \tag{21}$$

For F_h considerably lower than $F_{h_{crit}}$, the motion is dominated by the stratified cascade, and for F_h considerably larger that $F_{h_{crit}}$, the motion is dominated by the three-dimensional turbulence cascade. As for the maximum horizontal and vertical wavenumbers for which the hypothesis can be applied, we can now estimate them as

$$k_{h_{max}} \sim F_{h_{crit}}^{3/2}\, 2\pi/l_O, \qquad k_{v_{max}} \sim F_{h_{crit}}^{1/2}\, 2\pi/l_O. \tag{22}$$

We shall not think of three-dimensional turbulence as homogeneously distributed in space; on the contrary, it is very intermittently distributed. It is well known that three-dimensional turbulence prevails in extended pancake-shaped domains or blinis in the atmosphere as well as in the ocean. For this reason, it is difficult to determine experimentally an exact wavenumber where the transition takes place. This is true for the horizontal as well as the vertical wavenumber. For the horizontal spectrum we have used the observations of Vinnichenko (1970) to estimate the critical Froude number and thereby the typical transition wavenumber. As for the vertical spectrum, measurements of Alisse & Sidi (2000) indicate that the transition from a k_v^{-3} to a $k_v^{-5/3}$ spectrum in the atmosphere takes place in the wavenumber range corresponding to about 10 m. This is consistent with the estimate (22), since, with our estimated values of ϵ and N, the Ozmidov length scale is about 3 m. However, owing to the intermittent distribution of three-dimensional turbulence, there is no visible transition in one and the same measured spectrum. Some of the spectra in this wavenumber range show a k_v^{-3}-dependence and some of them show a $k_v^{-5/3}$-dependence.

3. Simulations

In order to simulate a low-Froude-number cascade in a box with periodic boundary conditions, just as is common practice for isotropic turbulence without stratification, the relation (7) suggests that it would be appropriate to use a box which is much larger in the horizontal direction than in the vertical direction, rather than a cubic box. If L_x is the length of a horizontal side of the box, we can set the vertical side length, L_z, so that $L_z/L_x \sim F_h$. This is simply because the height of the box does not need to be much larger than the largest vertical physical length scale that will develop in the box. On the other hand, we should also have

$$l_v/\eta_v \gg 1, \tag{23}$$

where η_v is the vertical diffusion length scale. As we will see, a characteristic feature of the motion we will simulate is the formation of layers. This strong tendency to layer formation was discovered by Herring & Métais (1989) in simulations of forced stably stratified turbulence. The layer thickness, which can be identified with l_v, will become thinner as we decrease the Froude number. If for a fixed l_h we decrease the Froude number without a corresponding decrease in the vertical diffusion length scale, the layers will soon become comparable to the diffusion length scale. In this way we will enter into the low-Reynolds-number regime by just increasing the strength of the stratification, without making any change to the total number of computational points. With Navier–Stokes diffusion, the diffusion length scale is equal in the vertical and horizontal directions, that is the Kolmogorov scale $\eta = \nu^{3/4}/\epsilon^{1/4}$. From Taylor's estimate (6), the classical relation $l_h/\eta \sim Re_h^{3/4}$ follows, where $R_h = ul_h/\nu$ is the Reynolds number based on the horizontal length scale. If n_h is the number of computational points required in each horizontal direction, then the number of points required in the vertical direction is $n_v \sim n_h F_h$ and the total number is $n_h^3 F_h \sim Re_h^{9/4} F_h \sim Re_v^{9/4} F_h^{-5/4}$, where Re_v is the Reynolds number based on l_v. In arriving at the last relation we have used (7). With $l_v \sim 1\,\mathrm{km}$, $u \sim 3\,\mathrm{m\,s^{-1}}$ and $\nu \sim 3 \times 10^{-5}\,\mathrm{m^2\,s^{-1}}$, we have $R_v \sim 10^8$ in the atmosphere. It is evident that even if Re_v were several orders of magnitude smaller, it would be impossible to reach the low-Froude-number regime using Navier–Stokes diffusion. With $F_h = 10^{-3}$ and thirty million computational points, we would have to choose $R_v < 100$. The flow would be controlled by viscosity to a very strong degree. We can see only one way out of this dilemma and that is to modify the diffusion terms

in (1)–(2), in a way that will permit us to decrease the vertical diffusion length scale as we increase the strength of the stratification, without any change of the horizontal diffusion length scale. Thus, we replace the diffusion operator in (1) with

$$-\nu_h \Delta_h^4 - \nu_v \frac{\partial^8}{\partial z^8}, \tag{24}$$

where Δ_h is the horizontal Laplace operator. The use of the higher-order differential operators in (24) has the advantage of narrowing the wavenumber band in which dissipation is important. The different diffusion coefficients permit us to use a grid for which the horizontal resolution is larger than the vertical resolution, that is $\Delta x = c\Delta z$ where $c > 1$. The ratio between the number of resolution points in the horizontal and the vertical directions should now be $n_h/n_v \sim 1/cF_h$. By permitting the scale factor c to increase, that is by stretching the grid, as we let F_h decrease, we can, for a given n_v, go to the limit of small F_h, without increasing n_h beyond all practical limits. However, there must be a lower limit to how small the ratio $\Delta z/\Delta x$ should be. This limit can be determined by the degree of anisotropy we can expect at the smallest resolved scales. As we will see, Δz will in general be chosen as a little larger than the Ozmidov length scale l_O. For the simulations with strongest stratification we will choose $\Delta z \approx l_O F_{h_{crit}}^{-1/2} = 7l_O$, so that the corresponding vertical cutoff wavenumber will be approximately equal to the value we estimated for $k_{v_{max}}$. This choice is motivated by our interest in the dynamics of scales larger that l_O which are strongly influenced by stratification. According to (22), at the smallest resolved scales the degree of anisotropy can thus be estimated as $k_{h_{max}}/k_{v_{max}} \sim F_{h_{crit}} \approx 0.02$. Thus, we should take $\Delta z/\Delta x \geqslant 0.02$. In the simulation with strongest stratification (run 10), we have not pushed this limit since we used $\Delta z/\Delta x = 1/24$. The shortcoming of the method of taking $\Delta z/\Delta x \ll 1$ is that three-dimensional overturning motions arising from Kelvin–Helmholtz instabilities in regions with strong vertical shear will not be well resolved. Riley & deBruynKops (2003) observed that such instabilities occur even in strongly stratified flows if the Reynolds number is sufficiently high. In this study, the resolution is generally sufficient to capture the horizontal breaking of shear layers that such instabilities generate, but not, in all cases, enough to resolve the fine structure of the flow field where these instabilities appear.

In equation (2), an expression corresponding to (24) is introduced, including a horizontal and a vertical diffusivity, κ_h and κ_v. In Fourier space, the expression corresponding to (24) is

$$-\nu_h \left(k_x^2 + k_y^2\right)^4 - \nu_v k_z^8. \tag{25}$$

The dissipation of kinetic and potential energy are exactly calculated as

$$\epsilon_K = \sum \left(\nu_h \left(k_x^2 + k_y^2\right)^4 + \nu_v k_z^8\right) \hat{\boldsymbol{u}} \cdot \hat{\boldsymbol{u}}^\star, \tag{26}$$

$$\epsilon_P = \sum \left(\kappa_h \left(k_x^2 + k_y^2\right)^4 + \kappa_v k_z^8\right) \hat{\phi}\hat{\phi}^\star, \tag{27}$$

where the hat denotes the Fourier transform, the star denotes the complex conjugate and the summation is taken over all wavenumbers. The Fourier transform is defined as

$$\hat{\boldsymbol{u}}(k_x, k_y, k_z) = \frac{1}{L_x L_y L_z} \int_0^{L_x} \int_0^{L_y} \int_0^{L_z} \boldsymbol{u} \exp(\mathrm{i}(k_x x + k_y y + k_z z))\, \mathrm{d}x\, \mathrm{d}y\, \mathrm{d}z. \tag{28}$$

To simulate a stationary cascade, we must introduce some kind of forcing, injecting energy into the system at a rate P. It is desirable that P is perfectly controllable,

so that it can be verified that the dissipation is equal to the energy injection, i.e. $\epsilon = P$. In this case, it is also desirable that the forcing does not introduce any vertical length scale into the system, since we would like to check the relation (7) as far as we can. Thus, if the forcing has a characteristic horizontal length scale l_h, but no characteristic vertical length scale, we would like to check that, for a given F_h, structures with vertical length scale l_v will be generated. This could be accomplished by letting the forcing be restricted to horizontal modes, i.e. to modes for which the vertical wavenumber, k_z, is zero. However, with such forcing, modes for which $k_z \neq 0$ will never grow if they are initially zero. Since we use zero initial fields, we require some additional weak forcing in vertical modes to trigger the development of vertical gradients. We would also like to avoid a forcing which imposes a preferred time scale into the system. The natural time scale which should develop by itself, is the eddy-turnover time scale, (20), independently both of which value we use for N and the kind of forcing we use. We would also like to check, independently of the forcing, that the amount of potential energy will become independent of F_h for small F_h, and that the energy content in the vertical velocity component will decrease as

$$E_w = \tfrac{1}{2}\langle ww \rangle \sim F_h^2 E_K, \tag{29}$$

as we decrease F_h.

To meet all the desired requirements as far as possible, we introduce a random white-noise forcing exclusively to the horizontal velocity equations, injecting energy into the system at a rate P. The forcing is divided into two parts, the main part being truly two-dimensional, i.e. it is not only restricted to the two horizontal velocity components, but also restricted to Fourier modes for which $k_v = 0$. We let this part of the forcing be responsible for 99 % of the energy injection. It has a two-dimensional spectrum

$$S_f(k_\rho) = k_\rho \exp((k_\rho - k_f)^2), \tag{30}$$

where k_f is the wavenumber around which the forcing is concentrated and $k_\rho = \sqrt{k_x^2 + k_y^2}$. The spectrum is normalized so that

$$\int_0^\infty S_f(k_\rho)\, \mathrm{d}k_\rho \Delta t = 0.99P, \tag{31}$$

where Δt is the time step. This procedure will guarantee that the required amount of energy is injected. Numerical fluctuations of the injection rate are avoided by using a similar method to that developed by Alvelius (1999). The 1.0 % of the energy which is not injected into horizontal modes is instead injected into the three modes for which $k_z = (3, 4, 5) \times 2\pi/L_z$ and $k_x = k_y = 0$. This part of the forcing is introduced to trigger the development of vertical gradients, which is necessary for the energy to spread from the horizontal to the vertical modes. The energy injection in each of these three modes is $P/300$ and is equally distributed over the two horizontal velocity components. With this type of forcing, the horizontal length scale is determined by k_f and can be set to $l_h = 2\pi/k_f$, while it can be assumed that the forcing in the vertical modes is sufficiently weak for the vertical length scale to develop independently of the forcing. In order for energy to spread to all modes, we must force at least two vertical wavenumbers, one odd and one even. The particular choice we made was motivated by our wish to leave the large vertical wavenumbers undisturbed and at the same time not to introduce forcing at the very smallest wavenumbers corresponding to the height of the box. However, it does not really matter what wavenumbers we choose. The result will essentially be the same, as long as the vertical forcing is weak. We have made several tests with forcing in different wavenumbers to investigate this. We

have also injected only one thousandth of the total energy into vertical modes, with essentially the same result. The difference is that the transition to a stationary state will be somewhat delayed using such a weak vertical forcing. As we shall see, it is also possible to shut off the vertical forcing once the vertical structures have developed.

We make a series of direct numerical simulations of the Boussinesq equations (1)–(3) where the diffusion terms have been modified and forcing has been added in the specified ways. The boundary conditions are periodic. Six runs are carried out in a $256^2 \times 32$ box, two runs are carried out in a $512^2 \times 32$ box, one in a $512^2 \times 64$ box and one in a $768^2 \times 48$ box. Starting from zero initial fields, the equations are solved using a standard pseudospectral code and a second-order four-step Runge–Kutta scheme with adaptable time step. The time step is limited by a stability condition, as described in Lundbladh *et al.* (1999). Full dealiasing according to the 3/2-rule is used in all simulations except the two largest (runs 9 and 10). The number of grid points is given in physical space, which means that the total number of Fourier modes used to calculate the nonlinear terms is a factor 27/8 larger in the eight runs in which we have used dealiasing.

The values of the diffusion coefficient are determined to obtain a state in which the injected energy is dissipated at the smallest resolved scales Δx and Δz. With the modification of the viscous terms, the horizontal dissipation length scale or 'Kolmogorov scale' can be estimated as $\eta_h = (\nu_h/\epsilon^{1/3})^{3/22}$, with a corresponding expression for the vertical dissipation length scale. Thus, we should have

$$\nu_h = \kappa_h = (a\Delta x)^{22/3} P^{1/3}, \tag{32}$$

where a is a constant, and a corresponding expression for $\nu_v = \kappa_v$, in which Δx is replaced by Δz. It was found that $a = 0.75$ was sufficient to resolve accurately the peaks in the dissipation spectra.

The series of simulations is performed as follows. The horizontal sides of the box are set to $L_x = L_y = 2\pi$. The energy injection is put to $P = 1$ and the horizontal forcing wavenumber is always $k_f = 4$ with the corresponding forcing length scale $l_h = \pi/2$. The Froude number $F_h = P^{1/3}/Nl_h^{2/3}$ is varied by varying N. First, we make a run (number 1) in a box with $L_z/L_x = 1/8$ and equal horizontal and vertical resolution, $\Delta x = \Delta z$. After some trial and error we found that $N = 12$ was an appropriate value to use in this simulation, corresponding to $F_h = 0.0617$. With this value we could see that structures developed with vertical length scale smaller than the height of the box and at the same time larger than Δz. The Froude number of this run is somewhat higher than the value we have estimated for $F_{h_{crit}}$. For run numbers 2–5 we then halve the Froude number step by step by increasing N by a factor of two for each run. At the same time, we halve the ratio L_z/L_x. Runs 6–10 will be discussed after the presentation of runs 1–5. For runs 1–5 we use $\nu_h = \kappa_h = 1.89 \times 10^{-13}$. The simulation parameters are given in table 1.

4. Results

In figure 3, we have plotted the normalized total energy $E/(Pl_h)^{2/3}$ and the normalized potential energy $E_P/(Pl_h)^{2/3}$ versus normalized time, $\tilde{t} = t/\tau = tP^{1/3}/l_h^{2/3}$, for runs 1–5. As we can see, after an initial linear growth of energy, there is a transition starting at approximately $\tilde{t} = 1$, to a statistically stationary or quasi-stationary state. In run 5, there is a slow growth of energy in the interval $10 < \tilde{t} < 20$, corresponding to 2 % of the energy injection P, which means that $\epsilon \approx 0.98P$ in this interval. The system can still can be regarded as being in a quasi-stationary state in this interval.

Run	F_h	$\frac{L_x}{L_z}$	$\frac{L_x}{\Delta x}$	$\frac{\Delta x}{\Delta z}$	$\frac{\Delta z}{l_O}$	$\nu_h = \kappa_h$	$\nu_v = \kappa_v$	$No \times 10^{-4}$	$\Delta t P^{1/3}/l_h^{2/3}$
1	6.17×10^{-2}	8	256	1	1.02	1.89×10^{-13}	1.89×10^{-13}	5	1.9×10^{-3}
2	3.08×10^{-2}	16	256	2	1.44	1.89×10^{-13}	1.17×10^{-15}	2	1.6×10^{-3}
3	1.54×10^{-2}	32	256	4	2.05	1.89×10^{-13}	7.27×10^{-18}	4	1.2×10^{-3}
4	7.71×10^{-3}	64	256	8	2.89	1.89×10^{-13}	4.51×10^{-20}	4	1.1×10^{-3}
5	3.85×10^{-3}	128	256	16	4.08	1.89×10^{-13}	2.80×10^{-22}	6	8.0×10^{-4}
6	6.17×10^{-2}	128	256	16	0.06	1.89×10^{-13}	2.80×10^{-22}	5	
7	3.85×10^{-3}	128	512	8	4.08	1.17×10^{-15}	2.80×10^{-22}	5	5.3×10^{-4}
8	1.93×10^{-3}	128	512	12	7.69	7.84×10^{-16}	6.97×10^{-24}	3	3.7×10^{-4}
9	1.93×10^{-3}	96	512	12	7.69	7.84×10^{-16}	6.97×10^{-24}	4	3.7×10^{-4}
10	9.64×10^{-4}	384	768	24	7.25	4.29×10^{-17}	3.71×10^{-27}	6	2.2×10^{-4}

TABLE 1. Simulation parameters. No is the number of time steps and Δt is the time step in the statistically stationary state. For run 6 no stationary state was reached and the time step was therefore decreasing during the whole run.

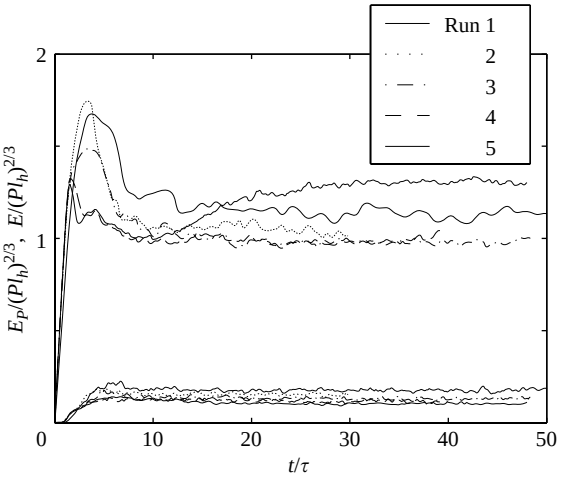

FIGURE 3. Time evolution of normalized total energy and potential energy. The solid curve showing a slow increase of total energy in the interval $10 < \tilde{t} < 20$ is from run 5.

However, the slow energy growth should make us cautious of trying to push the Froude number to even lower values. The reason behind it will be discussed in § 4.1. The transition beginning at $\tilde{t} = 1$ is seen in all runs and is fastest for runs 4 and 5 with lowest F_h. The transition is from a state determined by the forcing, in which there is practically no vertical variation, to a state in which there are layers separated by strong vertical gradients. Figure 4(a) is a contour plot, in a vertical plane, of the horizontal velocity component parallel to the plane at $\tilde{t} = 1$, from run 1. As we can see, there is still very little vertical variation. The field is dominated by the random forcing. In figure 4(b), we see the same field from run 1, in the state when the energy has reached a stationary level. Now there are layers separated by strong vertical gradients. In figure 4(c), the fluctuating temperature field is plotted in a vertical plane and again we see the layered structure. Contour plots of the velocity and temperature fields from runs 2–5, look very similar to the plots in figures 4(b) and 4(c), if the vertical sides of the boxes are stretched to the same length in the plots.

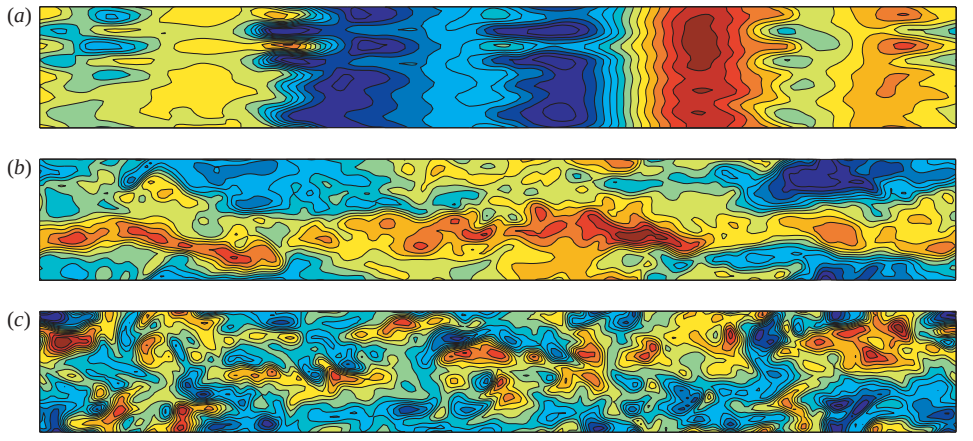

FIGURE 4. Contours in a vertical plane of (*a*) the horizontal velocity component parallel to the plane at $\tilde{t} = 1$, (*b*) the horizontal velocity component parallel to the plane in the statistically stationary state, and (*c*) the fluctuating temperature in the statistically stationary state, from run 1. $L_z/L_x = 1/8$.

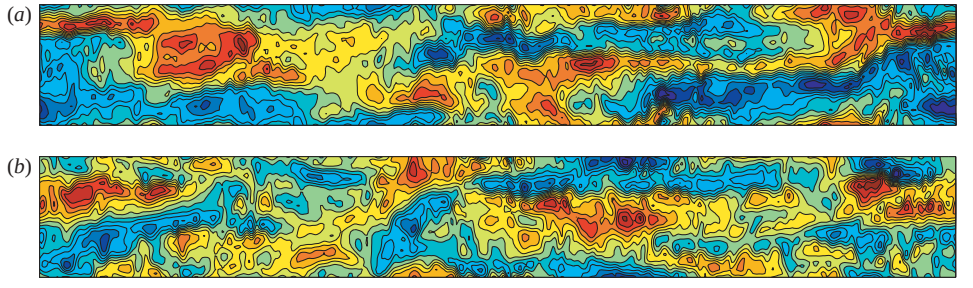

FIGURE 15. Contours in a vertical plane of (*a*) the horizontal velocity component parallel to the plane and (*b*) the fluctuating temperature, from run 8. The vertical side of the box is magnified by a factor of 24 in the figures. In the simulation, $L_z/L_x = 1/192$, while in the figure, $L_z/L_x = 1/8$.

In figure 5, we have plotted the normalized total dissipation ϵ/P and the normalized dissipation of potential energy ϵ_P/P versus $\tilde{t}$ for runs 1–5. As can be seen, there is a balance between energy input and dissipation during the whole runs except in the initial phase. Since the energy input is at large scales and the dissipation takes place at small scales, we can conclude that there is an energy cascade from large to small scales. In this case, there is also a considerable transfer of energy from kinetic to potential energy. Since we have chosen to restrict the energy input P to be in the form of kinetic energy this transfer is exactly equal to ϵ_P. This transfer is, of course, not a universal feature of the motion, but is due to the type of forcing we have used. In figure 5, we see that there is a small, but significant, decrease of ϵ_P/P, from run 1 to run 5. As seen in figure 3, there is also a corresponding slow decrease of potential energy E_P from run 1 to run 5. We do not speculate about the reason for this small decrease, but note that $\epsilon_P/\epsilon_K \approx 1/3$ for run number 5, with the lowest Froude number. This is consistent with the estimates made by Lindborg & Cho (2001*b*) from lower stratospheric data.

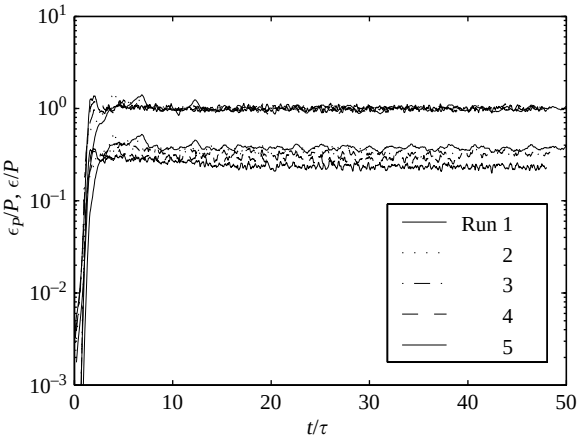

FIGURE 5. Time evolution of normalized total dissipation and dissipation of potential energy.

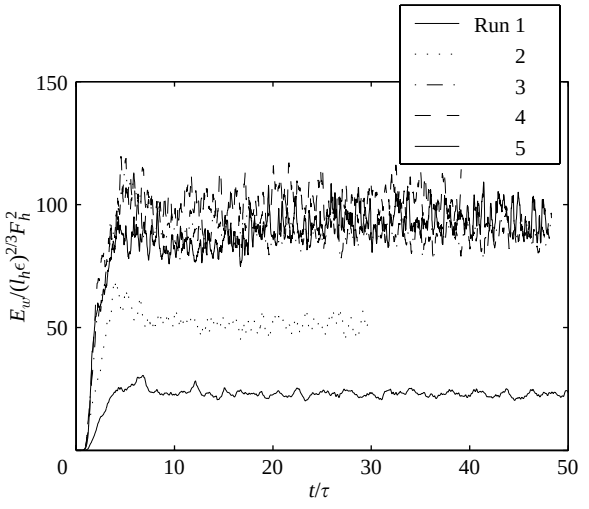

FIGURE 6. Time evolution of normalized energy content in the vertical velocity component. The lowest curve is from run 1.

We suggest that there is another universal feature to be seen in these simulations, in addition to the transfer of energy from large to small scales, and this is the transfer of energy from horizontal modes to vertical modes. Ninety nine per cent of the energy input is in modes for which $k_v = 0$. Energy is then transferred from these modes to modes for which k_v is large. From another point of view, this process can be described as a perpetual formation of layers. We suggest that this is a universal feature of strongly stratified flows in general.

While, according to our assumptions, the total kinetic and potential energy should be independent of the Froude number, the energy content in the vertical velocity component, E_w, should, according to (29), scale as $\sim F_h^2$. In figure 6, we have plotted $E_w/(F_h^2 P^{2/3} l_h^{2/3})$ versus $\tilde{t}$. As we can see, there is no similarity between the five runs. The curve for run 1, with the largest Froude number, is removed from the other curves. However, there is a good similarity between the three lowest Froude number runs. This is in line with what can be expected. For runs 1 and 2, F_h is a bit higher

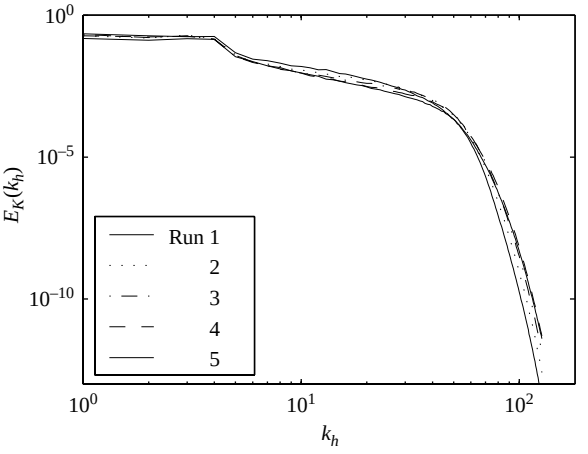

FIGURE 7. Horizontal kinetic energy spectra. The upper solid curve in the inertial range is from run 1, and the lowest curve is from run 5.

than the estimated critical value, while for runs 3–5 it is lower. We would like to emphasize that F_h^2 is varied by a factor of 1/256 from runs 1 to 5, while there is a variation by a factor of 5 between the normalized curves, so there is indeed a considerable variation of the absolute value of E_w. For run 5, the energy content in the vertical velocity component relative to the total energy is as small as 1.1×10^{-3}.

Before presenting the plots of the one-dimensional energy spectra, we should write down how we computed them. The one-dimensional horizontal kinetic energy spectrum was calculated as the mean value of the k_x and the k_y spectra,

$$E_{K_h}(k_h) = \tfrac{1}{2}\left[\frac{L_x}{2\pi}\sum_{\substack{|k_x|=k_h\\k_y,k_z}} \tfrac{1}{2}\hat{u}_i\hat{u}_i^\star + \frac{L_y}{2\pi}\sum_{\substack{|k_y|=k_h\\k_x,k_z}} \tfrac{1}{2}\hat{u}_i\hat{u}_i^\star\right], \tag{33}$$

and the one-dimensional vertical kinetic energy spectrum was calculated as

$$E_{K_v}(k_v) = \frac{L_z}{2\pi}\sum_{\substack{|k_z|=k_v\\k_x,k_y}} \tfrac{1}{2}\hat{u}_i\hat{u}_i^\star. \tag{34}$$

The one-dimensional potential energy spectra were calculated in a corresponding way.

In figure 7, we have plotted the one-dimensional horizontal spectra of kinetic energy for runs 1–5. The effect of the forcing is clearly visible in wavenumber $k_h = k_f = 4$. At the very highest wavenumbers the spectra are falling off rapidly to very small values, showing that the resolution is good enough with the given diffusion model. Between k_f and the dissipation range there is an intermediate range where we should look for a possible $k_h^{-5/3}$-dependence of the spectra. In figure 8, we have plotted the one-dimensional spectra of potential energy. Apart from wavenumbers smaller than k_f, the potential energy spectra look similar to those of the kinetic energy spectra. In figures 9 and 10, we have plotted the spectra in compensated form: $E_K(k_h)k_h^{5/3}/\epsilon_K^{2/3}$ in figure 9 and $E_P(k_h)k_h^{5/3}\epsilon_K^{1/3}/\epsilon_P$ in figure 10. For the highest Froude number runs, there are no clear power-law dependences of the spectra. However, it is clear that the spectra are approaching a $k_h^{-5/3}$-dependence as the Froude number is decreased. For

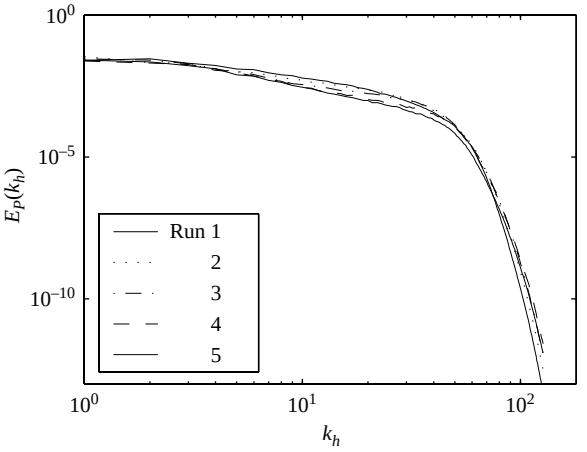

FIGURE 8. Horizontal potential energy spectra. The upper solid curve in the inertial range is from run 1, and the lowest curve is from run 5.

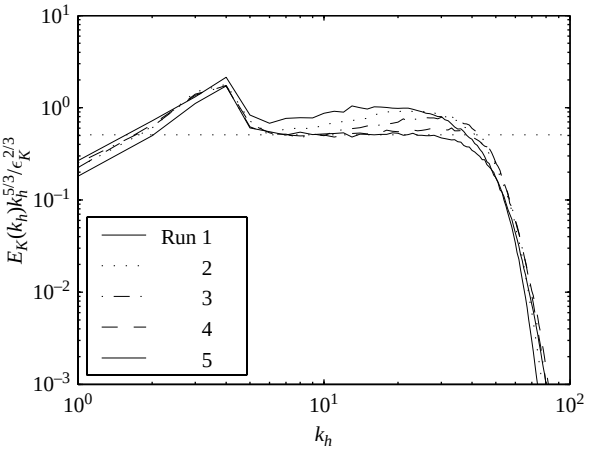

FIGURE 9. Compensated horizontal kinetic energy spectra. The upper solid curve in the inertial range is from run 1, and the lowest curve is from run 5. Dotted line, $C_1 = 0.51$.

run 5, with the lowest Froude number, the compensated spectra fall on straight lines. Writing the power laws as

$$E_{K_h}(k_h) = C_1 \epsilon_K^{2/3} k_h^{-5/3}, \tag{35}$$

$$E_{P_h}(k_h) = C_2 \frac{\epsilon_P}{\epsilon_K^{1/3}} k_h^{-5/3}, \tag{36}$$

where C_1 and C_2 are constants, from figure 9 and 10 we can estimate the constants to $C_1 \approx 0.51$ and $C_2 \approx 0.51$. Within the given numerical accuracy, we find that they have the same value. In this study, we will not speculate about the reason for this, but leave it as a challenge for future investigators to explain.

In principle, we could have written the power laws using only the total dissipation, ϵ, as the scaling parameter, that is in the form $E_{K_h}(k_h) = C_1' \epsilon^{2/3} k_h^{-5/3}$ and $E_{P_h}(k_h) = C_2' \epsilon^{2/3} k_h^{-5/3}$ where C_1' and C_2' are other constants. If the ratio ϵ_P/ϵ_K is a universal constant, then C_1' and C_2' have the same degree of universality as C_1 and

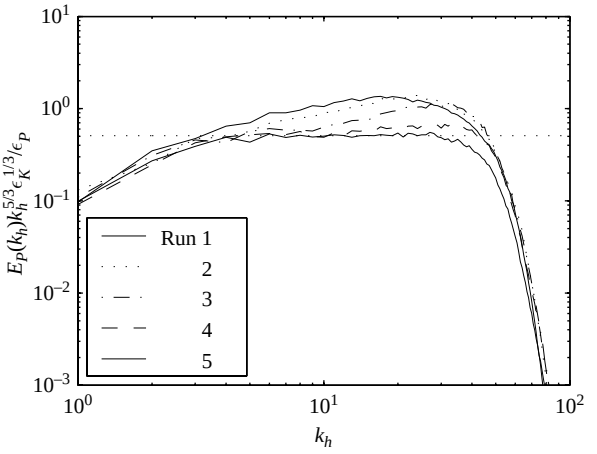

FIGURE 10. Compensated horizontal potential energy spectra. The upper solid curve in the inertial range is from run 1, and the lowest curve is from run 5. Dotted line, $C_2 = 0.51$.

C_2. However, it was found in the companion paper (Lindborg 2005), that the ratio ϵ_P/ϵ_K tends to increase somewhat in the presence of system rotation, and that the most general expressions of the scaling laws are (35) and (36).

The approach of the spectra towards a $k_h^{-5/3}$-power law is in full agreement with the hypothesis presented. The Froude numbers of runs 1 and 2 are both a bit higher than the value we estimated for $F_{h_{crit}}$. There is a general similarity between these two runs and the other three runs, in terms of the development of total energy and the energy dissipation. Obviously, there is also a forward cascade taking place in these runs. However, there is no clear power-law dependence of the spectra in these runs. This should be explained by the fact that we are in a transition region between two different modes of motion: the strongly stratified cascade and the classical three-dimensional Kolmogorov cascade. In this transition region, there is no clear power-law dependence. By decreasing the Froude number, we obtain a clear approach to (35) and (36).

We now turn to the one-dimensional vertical spectra. Since only 32 points were used in the vertical direction, these spectra are rather narrow. For this reason, we will not look for any power-law range, but only investigate to what extent the spectra conform to the similarity expressions (12) and (13). In figure 11, the scaled kinetic and potential energy spectra for runs 1–5 are plotted, $E_{K_v}/u^2 l_v$ (solid lines) and $E_{P_v}/u^2 l_v$ (dashed lines) versus the scaled vertical wavenumber $k_v l_v$, where l_v has been calculated according to (16). As we can see, there is a reasonable collapse of the kinetic energy spectra, except for the dissipation range, where such a collapse should not be expected. As for the potential energy spectra there is a minor decrease in magnitude with decreasing F_h, reflecting the fact that there was a minor decrease of total potential energy with the increasing degree of stratification from run 1 to run 5. However, given that F_h as well as the box height were decreased by a factor of 16 from run 1 to run 5, we find the collapse to be reasonable also for the potential energy spectra.

On the whole, the results from runs 1–5 are in general agreement with the hypothesis presented. A forward stationary energy cascade was seen in all runs, a cascade of both kinetic and potential energy. A reasonable similarity of global measures was seen between all five runs and a reasonable similarity of the spectra was seen between

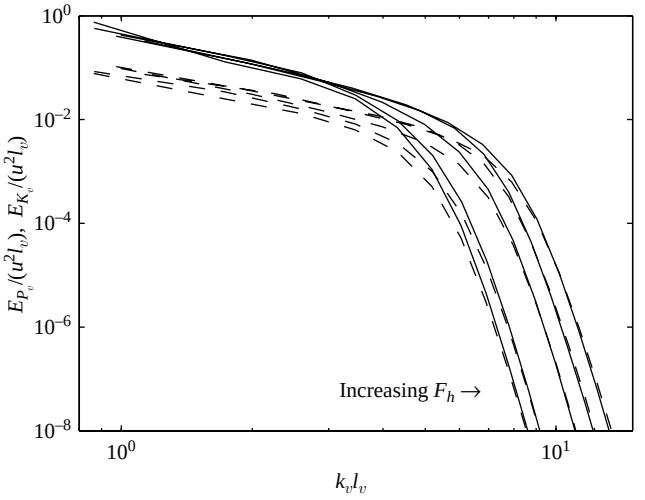

FIGURE 11. Normalized vertical kinetic (solid lines) and potential (dashed lines) energy spectra for runs 1–5. In the dissipation range, we see the spectra from run 1 to run 5 from right to left, with F_h increasing in the opposite direction.

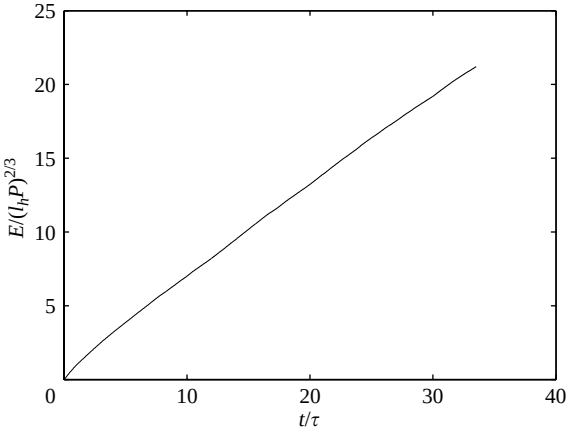

FIGURE 12. Time evolution of normalized total energy from run 6.

runs 3 and 5, with the lowest Froude numbers. Moreover, a $k_h^{-5/3}$-range was seen for the horizontal energy spectra.

4.1. *Runs* 6–10

In runs 1–5 we have adjusted our parameters so that $L_z/L_x \sim F_h$. In fact, we have $L_z/L_x = 2.03F_h$ in all five runs. We now ask, 'What would happen in a simulation with $L_z/L_x \ll F_h$?' In this case, the energy which is fed into the horizontal modes with characteristic length scale l_h, cannot be transferred to modes with characteristic vertical length scale $l_v \sim F_h l_h$, because there are no such modes. Therefore, energy must accumulate in the horizontal modes and a stationary state will never be reached. Energy will continue to grow. To test whether this is what happens, we have run a simulation (run 6) with $F_h = 0.0617$ and $L_z/L_x = 1/128 = 0.13F_h$. The parameters of run 6 are given in table 2. In figure 12, we have plotted the evolution of the

total energy for run 6. Indeed, there is a continuous growth of energy through the whole simulation. Kinetic energy is accumulated in the same horizontal modes as it is introduced to by the forcing, while the growth of potential energy is negligible. We find this test to be of crucial importance for the consistency of the present hypothesis.

As we pointed out, there is a slight difference between the energy evolution of run 5, as seen in figure 3, and the rest of the runs. For this run, the energy curve is not levelling out as fast and as completely as in the other runs. In the interval $10 < \tilde{t} < 20$, there is a slow growth of energy corresponding to 2 % of P, and the energy is levelling out at a somewhat higher value. A closer inspection shows that the energy accumulation in run 5, is in purely vertical modes, i.e. modes for which $k_\rho = 0$. These modes correspond to layers filling the whole box. A similar energy accumulation has been observed in small-scale forced box simulations of the Boussinesq equations by Smith & Waleffe (2002) and large-scale forced simulations by Laval, McWilliams & Dubrulle (2003) and Waite & Bartello (2004). In the Appendix, we discuss the possible reasons behind this phenomenon and suggest that the main reason is that when the layers are becoming so thin that they are comparable with the diffusion length scale, they also become stabilized and do not break up in the horizontal. In other words, we think it is a low-Reynolds-number effect which can be avoided by decreasing the influence of diffusion, which normally requires increased resolution. To support this hypothesis, we have run three simulations with different vertical diffusion coefficients, showing that the growth in $k_\rho = 0$ modes increases with increased vertical diffusion. These are presented in the Appendix. Here, we proceed by investigating whether the slow energy growth in $k_\rho = 0$ modes can also be avoided by decreasing the horizontal diffusion coefficients, which requires increased horizontal resolution. At the same time, we will investigate whether a broader $k_h^{-5/3}$-range can be obtained in this way.

First, we make two further runs with doubled resolution in the horizontal direction as compared to run 5. In the first of these runs (run 7), the parameters are the same as in run 5, except for $\Delta x/L_x$ and ν_h. In run 8 we halve the Froude number as compared to runs 5 and 7, and at the same time decrease the ratio L_z/L_x by a factor of 2/3, so that $L_z/L_x = 1/192$. In run 8, we also use somewhat lower values of the constant a in (32) to determine the diffusion coefficients. Then, we also make another simulation (run 9) to show that our general results are independent of the height of the box. The principal difference we should see by increasing the box height is a corresponding increase of the number of layers. In principle, we should be able to produce the same kind of results in cubic boxes as in our very elongated boxes, however, at a much higher computational cost. In run 9, we take the more modest route of increasing the box height by a factor of two as compared to run 8, leaving all other parameters unchanged. This means that $L_z/L_x = 1/96$ in this run and that the number of grid points is 64×512^2 as compared to 32×512^2 in runs 7 and 8. In run 9, we introduce the weak perturbation forcing in the vertical modes $k_z = (6, 7, 8) \times 2\pi/L_z$, as compared to $k_z = (3, 4, 5) \times 2\pi/L_z$ in the other runs, so that the perturbation has approximately the same absolute scale when we have doubled L_z. We also shut off this weak forcing after 8000 of a total of 40 000 time steps, and instead inject 100 % of the energy into the purely horizontal modes. We do this to show that the perturbation forcing is important only to introduce the initial layering and once this has been done, the layer formation will continue without this weak perturbation. In figure 13, we can see the energy evolution from runs 7–9 and also run 10 which will be discussed below. As we can see, there is no slow energy growth visible in this plot. This is in agreement with the arguments we developed above. By decreasing the horizontal diffusion length scale

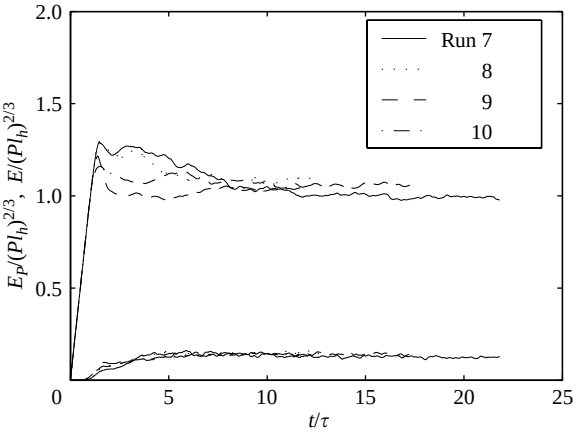

FIGURE 13. Time evolution of normalized total energy and potential energy.

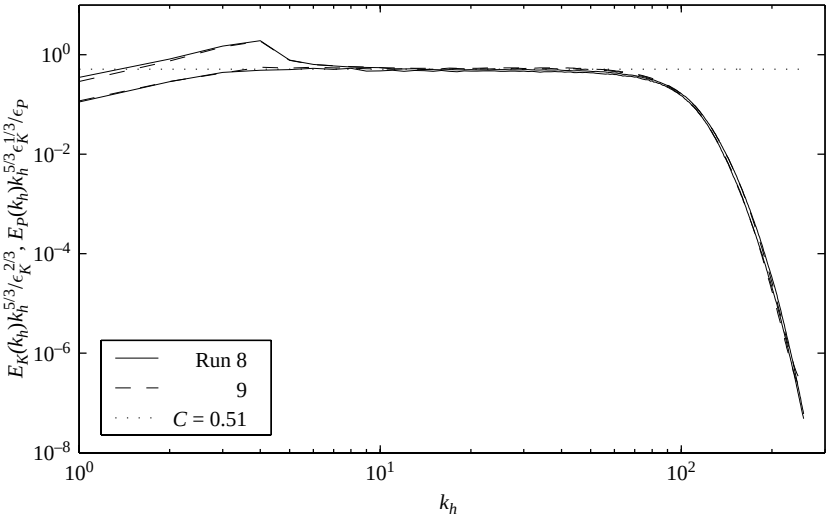

FIGURE 14. Compensated horizontal kinetic and potential energy spectra from runs 8 and 9.

η_h in runs 7–9. as compared to run 5, we have avoided the slow energy accumulation in the modes for which $k_\rho = 0$.

In figure 14, we have plotted the compensated kinetic and potential energy spectra from runs 8 and 9. The spectra are computed as time averages over five different spectra taken at intervals of approximately one eddy turnover time. There is a one decade long range where spectra are in good agreement with (35) and (36) and, as far as we can see, the two constants take the same value: $C_1 \approx C_2 \approx 0.51$. For both of the runs, we calculated ϵ_K and ϵ_P as time averages over the same total time interval as the spectra were taken from, and found that $\epsilon_K = 0.71$ and $\epsilon_P = 0.29$ in both cases. From the results from runs 8 and 9, we can conclude that we have used sufficiently high boxes.

To illustrate the layer-formation process, we present contour plots in a vertical plane, from run 8, of the horizontal velocity component parallel to the plane in

figure 15(*a*) and the temperature field in figure 15(*b*) (see page 219). In both plots, the vertical side of the box is magnified by a factor of 24 and in both plots we see the characteristic layered structure. We find it remarkable that this structure is developed in this extremely elongated box, in spite of the fact that virtually all energy is fed into modes with no vertical variation. In the presence of strong stratification, the energy which is fed into the modes for which $k_v = 0$, will spread to modes with large k_v, a process which is seen as layer formation. This process is so efficient that all energy which is fed into the large horizontal scales, is successively transferred to small scales where it is dissipated.

So far, we have concluded from the overall energy balance that there must be a cascade of energy from large to small scales, or, in other words, a spectral energy flux from small to large wavenumbers. To prove, beyond all doubt, that there is such a forward cascade we would like to quantify this spectral flux. However, since the vertical length scale is so much smaller than the horizontal length scale, we cannot use the standard definition for the spectral flux which is relevant in the case of isotropic turbulence (see e.g. Frisch 1995). In the present case, we would like to distinguish between the flux through horizontal wavenumbers, and the flux through vertical wavenumbers, and also to distinguish between the flux of kinetic energy and the flux of potential energy. To do this, we first define two spectral energy transfer functions as

$$T_K(k_x, k_y, k_z) = -\tfrac{1}{2}\mathrm{i}k_i(\hat{u}_j\widehat{u_i u_j}^\star - \hat{u}_j^\star\widehat{u_i u_j}), \tag{37}$$

$$T_P(k_x, k_y, k_z) = -\tfrac{1}{2}\mathrm{i}k_i(\hat{\phi}\widehat{u_i\phi}^\star - \hat{\phi}^\star\widehat{u_i\phi}), \tag{38}$$

with summation over repeated indices. If T_K is negative for a certain Fourier mode, it means that there is a transfer of kinetic energy from this mode and if T_K is positive it means that there is a transfer of kinetic energy to this mode from other regions in Fourier space. The sum of T_K over all Fourier modes is equal to zero, reflecting the fact that the nonlinear terms in equation (1) conserve kinetic energy. T_P has the corresponding properties, with respect to transfer of potential energy in Fourier space and the conservation of total potential energy by the nonlinear terms in equation (2). We now define the kinetic energy flux through horizontal wavenumber k_ρ as

$$\Pi_{K_h}(k_\rho) = -\sum_{\substack{\sqrt{k_x^2+k_y^2}\leqslant k_\rho \\ k_z}} T_K(k_x, k_y, k_z), \tag{39}$$

and the kinetic energy flux through vertical wavenumber k_v as

$$\Pi_{K_v}(k_v) = -\sum_{\substack{|k_z|\leqslant k_v \\ k_x, k_y}} T_K(k_x, k_y, k_z). \tag{40}$$

The corresponding fluxes of potential energy, $\Pi_{P_h}(k_\rho)$ and $\Pi_{P_v}(k_v)$, are defined in the corresponding way. Generally, a positive value of the flux functions means that there is a flux of energy from small to large wavenumbers, that is a forward cascade, and a negative value means that there is a flux in the other direction, that is an inverse cascade. A constant flux range is said to be an inertial range.

To compute these fluxes, we have performed one more simulation (run 10) in a $768^2 \times 48$ box. The side length ratio of the box was as low as $L_z/L_x = 1/384$ and

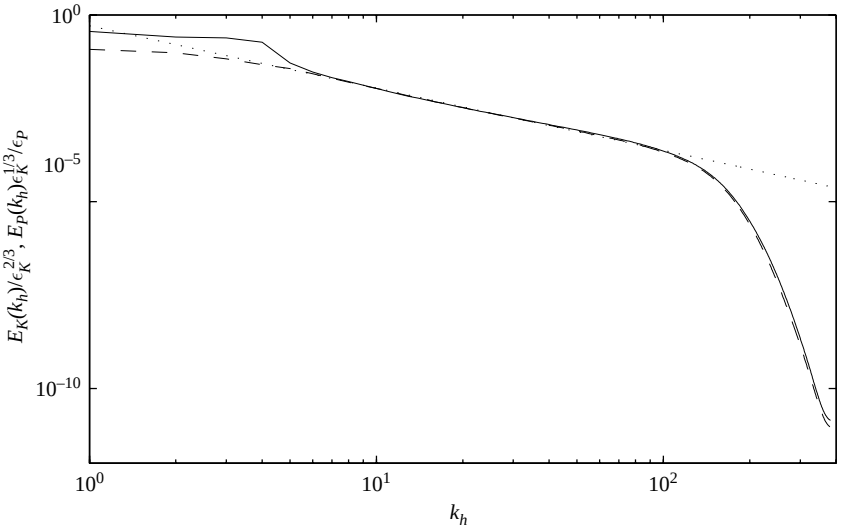

FIGURE 16. Normalized horizontal kinetic (solid curve) and potential (dashed curve) energy spectra from run 10. Dotted line, $0.51k_h^{-5/3}$.

the Froude number as low as $F_h = 0.00096$. Exactly the same kind of evolution of global parameters was observed as in the other runs: a fast transition beginning at $\tilde{t} \approx 1$ from an initial linear growth of energy to a statistically stationary state. The perturbation forcing was shut off after 20 000 of a total of 56 000 time steps and this caused essentially no change observed in any of the computed global quantities, nor in the spectra. The total energy injection was held constant by increasing the injection into horizontal modes from $0.99P$ to P when the perturbation forcing was shut off. The simulation was run for about twelwe eddy turnover times and the stationary values of the global parameters were: $E/(Pl_h)^{2/3} = 1.08$, $E_P/(Pl_h)^{2/3} = 0.14$, $\epsilon_K = 0.76$ and $\epsilon_P = 0.24$. The ratio between the energy content in the vertical velocity component and the total energy was as low as $E_w/E = 3 \times 10^{-4}$.

In figure 16, we see the horizontal kinetic and potential energy spectra from run 10. In this plot, we have averaged the spectra from eight different times separated by one eddy turnover time. The spectra are normalized according to (35) and (36) using $\epsilon_K = 0.76$ and $\epsilon_P = 0.24$, values calculated as time averages over the total time interval from which the eight spectra were taken. As we can see, there is a range over one decade long where both the curves fall onto the dotted line: $0.51k_h^{-5/3}$. Again we find that the two constants in (35) and (36) take the same value and with a reasonable error estimate we determine these constants to $C_1 \approx C_2 = 0.51 \pm 0.02$.

In figure 17, we see the vertical kinetic and potential energy spectra from run 10. To illustrate the large separation of vertical scale from horizontal scale, we have not normalized the vertical wavenumber in this plot. The smallest non-zero vertical wavenumber is $k_v = 384$ which is comparable with the largest horizontal wavenumbers. For comparison with equation (15), we have also inserted the curve $N^2k_v^{-3}$ (dashed line) in the figure. The spectra are still too narrow to distinguish any power-law range. If we looked for a power law, we would probably see something like k_v^{-m} with $2.3 < m < 3.0$, with the lower value for the potential energy spectrum. However, the interesting thing about these spectra is not the exact slope, but that

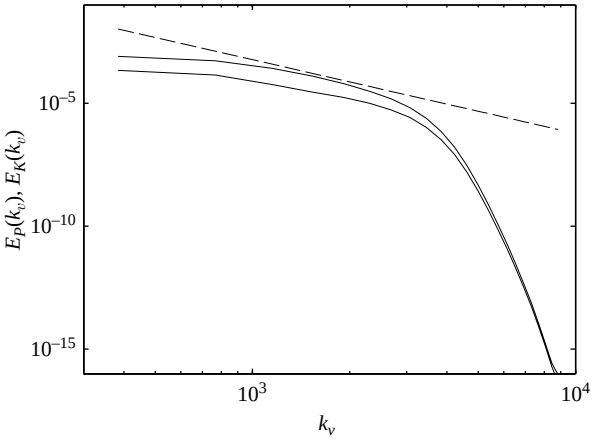

FIGURE 17. Kinetic (upper curve) and potential (lower curve) vertical energy spectra versus k_v from run 10. Dashed line, $N^2k_v^{-3}$.

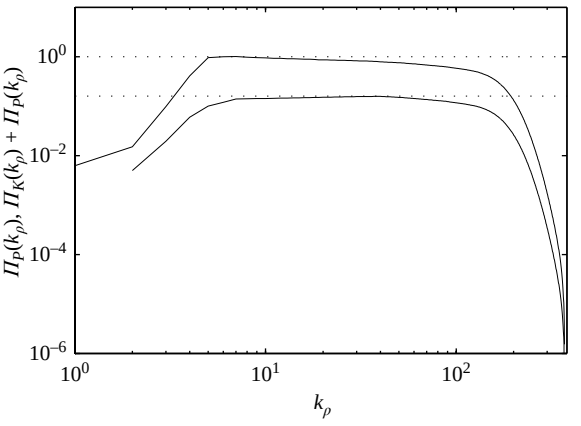

FIGURE 18. Total spectral energy flux (upper curve) and potential energy flux (lower curve), versus k_ρ, from run 10.

they are in the vicinity of the dashed line $N^2k_v^{-3}$. This result is consistent with scaling with N^2 in the limit of low Froude number and high Reynolds number.

In figure 18, we have plotted the spectral energy flux through the horizontal wavenumber k_ρ. The upper curve is the total flux and the lower curve is the potential energy flux. First, we note that both curves are generally positive, which means that there is a flux of kinetic and potential energy from low to high wavenumbers, i.e. a forward cascade. Next, we note that the total flux is approximately equal to unity from wavenumber $k_\rho = 5$, which is just one wavenumber larger than the forcing wavenumber $k_f = 4$, up to fairly large k_ρ. This means that all the injected energy flows in the direction of large k_ρ. In the middle range of wavenumbers, corresponding to the $k_h^{-5/3}$-range in figure 16, both curves show a nearly constant flux range. There might be an objection that the curves are not sufficiently close to constant values to justify the conclusion that there is a constant flux range. However, the same could be said about the corresponding flux curves calculated from high-Reynolds-number simulations of isotropic turbulence (Kaneda *et al.* 2003). These simulations show that the constant spectral flux range is approached very slowly with increasing Reynolds

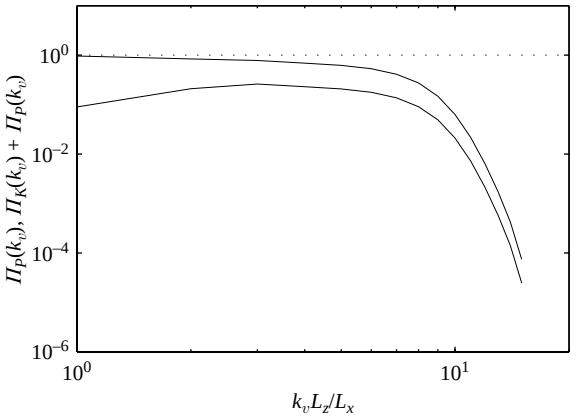

FIGURE 19. Total spectral energy flux (upper curve) and potential energy flux (lower curve), versus $k_v L_z/L_x = k_v/384$, from run 10.

number for isotropic turbulence. There is no reason to expect a different behaviour in the present case. Evidently, the $k_h^{-5/3}$-spectra in figure 16, can be interpreted as the energy spectra in a constant spectral flux range, just as the corresponding energy spectrum of three-dimensional turbulence.

In figure 19, we have plotted the energy flux through vertical wavenumber k_v. The upper curve is the total flux and the lower curve is the potential energy flux. In this plot, we have normalized the vertical wavenumber by $L_x/L_z = 384$, which means that the smallest non-zero vertical wavenumber corresponds to unity in the figure. As we can see, the total flux through this wavenumber is very close to unity. This means that all the energy which is injected in purely horizontal modes ($k_v = 0$) flows through this wavenumber, $k_v = 384$, in the direction of even larger vertical wavenumbers. As for the flux of potential energy, we can note that this function goes to zero for small k_v, owing to the fact that the potential energy was not forced. Instead, there is a transfer from kinetic to potential energy in the smallest vertical wavenumbers. This energy is then flowing in the direction of larger k_v and Π_{P_k} has a maximum around $k_v = 1152$, which is larger than the largest horizontal wavenumbers in figure 18. This is an extreme case of the highly anisotropic spectral energy flux through large vertical wavenumbers which was discovered by Godeferd & Cambon (1994) by investigating an EDQNM model for moderately stratified turbulence. In physical space, this flux manifests itself as layer formation.

4.2. *The length-scale ratio*

In figure 20, we have plotted the vertical to horizontal length-scale ratios l_v/l_h and l'_v/l_h versus F_h for all our runs, including run 6 in which no stationary state was reached. l_v and l'_v were calculated according to (16) and (17) using vertical spectra which were time averaged, except for run 6 where the spectra from the end of the simulation were used. As seen in the figure, both the length scale ratios follow a linear dependence on F_h, as indicated by the dashed lines. This is consistent with (7). Ideally, this relation should have been tested without decreasing the box height with decreasing F_h. However, with the computer resources which we have available this would not have been possible. The question is whether the linear dependence of l_v/l_h and l'_v/l_h on F_h seen in figure 20 is an artefact of the adjustment of the side length ratio of the box according to $L_z/L_x \sim F_h$. We will argue that this is not the case.

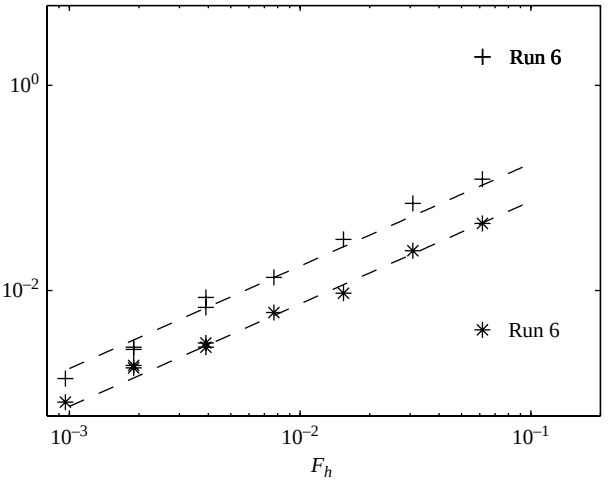

FIGURE 20. Length-scale ratios versus F_h for run 1–10. +, l_v/l_h; *, l'_v/l_h.

First of all, we note that for the runs giving statistically stationary solutions, the box side ratio has not been varied in exact proportion to F_h. We have $L_z/L_x = 2.03F_h$ in runs 1–5 and run 7, $L_z/L_x = 2.70F_h$ in runs 8 and 10 and $L_z/L_x = 5.41F_h$ in run 9. In particular, a comparison between runs 8 and 9, where L_z/L_x has been doubled in run 9 as compared to run 8, without any other change, indicates that the computed length scale ratios are not artefacts of the side length ratio of the box. The calculated length scale ratios were found to be $l_v/l_h = 0.0029, 0.0028$ and $l'_v/l_h = 0.0019, 0.0018$, for runs 8 and 9, respectively, which are practically the same values. This indicates that the box height is sufficiently large for the vertical length scale to develop inside the box. Secondly, the fact that we see a perfect balance between energy injection and dissipation indicates that the boxes are sufficiently high in each case. Virtually all energy is injected into modes for which $k_v = 0$ and is transferred to modes for which k_v is large. Had the boxes been too thin, all energy would not have been transferred in this way. Instead, energy would have grown in the $k_v = 0$ modes corresponding to length scales larger than the box height. This is also what happens in run 6 where $L_z/L_x = 0.13F_h$. In this run, kinetic energy is constantly growing in the $k_v = 0$ modes where it is injected and the length scale ratio l_v/l_h computed at the end of the simulation is in fact larger than unity, as seen in figure 20. In this case, the box is too thin for the vertical length scale to develop inside the box. The potential energy in this case reaches a stationary value and the potential energy fluctuations develop on the scale of the box height, which is reflected by the very low value of l'_v/l_h for run 6 seen in figure 20. However, this is more of a curiosity, since there is virtually no exchange from kinetic to potential energy and the amount of potential energy is less than one-thousandth of the amount of kinetic energy through the whole simulation. On the whole, we can conclude that our results are supporting the length scale relation (7) and thereby also the scaling (9) suggested by Billant & Chomaz (2001), since $F_v \sim l_h/l_v F_h \sim 1$. A direct calculation of $F_v = \sqrt{E_K}/Nl_v$ gives $F_v \approx 0.6$ for all the statistically stationary solutions. That $F_v \sim 1$ has also been observed in numerical simulations by Godeferd & Staquet (2003).

4.3. *Comparison with the results by Waite & Bartello*

Waite & Bartello (2004, hereinafter referred to as W & B) have performed a series of simulations of the Boussinesq equations which in some respects are similar to those presented here. W & B use a forcing which is restricted to purely horizontal modes ($k_v = 0$) with at sharp peak at $k_\rho = 3$ as compared to $k_\rho = 4$ which we have used. Instead of introducing a weak perturbation forcing in vertical modes, as we do, they start with non-zero random initial fields, ensuring that vertical structures will emerge. By shutting off the perturbation forcing in our runs 9 and 10 and continuing the simulations with forcing only in horizontal modes, we have shown that our results are not dependent on a continuous weak forcing in vertical modes, but only on the existence of an initial seed energy, as in their simulations. W & B also observe a strong tendency to layer formation, that is a strong growth in modes for which $k_v \gg k_\rho$, despite the fact that there is no forcing in modes for which $k_v \neq 0$. They also present evidence that the layer thickness scales as $l_v \sim u/N$, confirming the scaling suggested by Billant & Chomaz (2001). After the initial growth of energy, the W & B simulations are almost energetically stationary, a fact which is supporting the forward energy cascade hypothesis. Although they observe the same kind of weak growth in $k_\rho = 0$ modes as Smith & Waleffe (2002), they do not interpret this growth as a sign of an inverse energy cascade. On the other hand, they conclude that their results confirm the lack of an inverse cascade. So far, the results of our simulations and the simulations by W & B are very similar.

However, there are also important differences. First of all, W & B perform their simulations in a cubic box and the resolution scale is the same in the vertical and the horizontal directions. They also use hyperviscosity, however, with the same diffusion coefficients in the vertical and the horizontal directions. As they increase the strength of the stratification and the layer thickness decreases, the number of layers increases in the box. This is reflected in their one-dimensional vertical energy spectra which exhibit a long flat range from the smallest non-zero wavenumber, corresponding to the box height, to a wavenumber $k_v \sim N/U$, corresponding to the layer thickness. As shown by W & B, this flat range is just a mathematical consequence of the fact that the layer thickness l_v is the largest vertical physical length scale in the field and that l_v is much smaller than the box height. W & B demonstrate that the layers are dynamically decoupled from each other. This general result can, in fact, be used in support of our approach of using highly elongated boxes containing only a few layers. Having demonstrated that the fields decouple into a number of layers and that there are no larger vertical length scales than the layer thickness, it is computationally more economic to include only a small number of layers in the box. The reason why we do not see any long flat range in our vertical spectra is that the layer thickness is comparable to the box height in our simulations. Our vertical spectra instead reflect the dynamics within the thickest layers.

As the strength of the stratification is increased in the simulations of W & B, the whole flow field is stabilized. Contour plots in vertical planes reveal a number of smooth layers piled on top of each other, without much internal structure, in the vertical or in the horizontal directions. There are no instabilities or overturning motions visible as in the corresponding plots of fields with a weaker degree of stratification. We may interpret this stabilization as a mere consequence of the strong stratification. However, there is another interpretation which we find more plausible. As the layers are becoming thinner they ultimately become comparable to the resolution scale Δz, where diffusion is strong. This tends to stabilize the layers. With a thickness comparable to Δz they can, of course, no longer reveal any internal structure in the vertical

direction and they also become more resistant to instabilities that tend to break them up in the horizontal direction. The horizontal spectra of W & B exhibit a drop from an approximate $k_h^{-5/3}$-dependence at moderate stratification to an approximate k_h^{-5}-dependence at strong stratification. The whole spectrum becomes much steeper with much lesser energy content in high wavenumbers as the stratification increases. We interpret this as a consequence of the viscous stabilization of the layers which prevents them breaking up in the horizontal direction. In our simulations, we have avoided this stabilization by decreasing the vertical resolution scale as we increase the stratification, keeping the number of resolution points per layer approximately constant. Our contour plots of flow fields with a very strong degree of stratification exhibit layers with more internal structure and also breaking events. This is why our horizontal spectra do not show the sudden drop from $k_h^{-5/3}$ to k_h^{-5} as we increase the stratification.

5. Conclusions

Let us compare the extent of scales we have simulated in the largest simulation (run 10) with the mesoscales in the upper troposphere or lower stratosphere. Based on realistic values of N and ϵ, we estimated the Ozmidov length scale to be about 3 m. In run 10 we have chosen $\Delta z \approx 7l_O$, which would correspond to a vertical resolution of about 20 m. Since we used 48 points in the vertical direction, the box height would be about 1 km. The horizontal resolution would be $\Delta x \approx 500$ m and the width of the box would be about 400 km. The forcing scale would correspond to a scale of about 100 km and the $k_h^{-5/3}$ range we see in figure 16, would correspond to a range of wave lengths from 10 km to 100 km, where we actually do find the $k_h^{-5/3}$-range in figure 1. Although our range of scales is still limited, both in the vertical and horizontal, as compared to the real atmosphere, we are clearly in the correct domain. Our simulation model is, of course, in many respects extremely idealized and simplified. The boundary conditions are periodic, and the forcing is supposed to replace the prevalence of synoptic atmospheric motions capable of feeding energy into the mesoscale range, by some mechanisms similar to what we see in the zigzag instablity. Moreover, the very crude diffusion model is supposed to replace the action of classical three-dimensional turbulence on the mesoscale motions. At vertical scales around the Ozmidov length scale or a bit larger, classical three-dimensional turbulence will be produced and will act on the mesoscale motions in such a way that energy is further transferred all the way down to the Kolmogorov scale, $\eta \approx 1$ cm, where it is dissipated by molecular diffusion. It may be argued that much more understanding of the dynamics could be gained by also resolving this dynamically active range of scales, or at least a part of it. However, to make a substantial gain, we would probably need to resolve scales well below the Ozmidov scale on an isotropic grid, which would require an enormous increase in the number of computational points. As long as the number of computational points cannot be increased by several orders of magnitude, we think the most fruitful approach is, in fact, to introduce a rather sharp viscous cutoff at wavenumber $k_{v_{max}}$. If this is done, it can also be argued that the use of a highly stretched grid is justified.

Simplifications and idealizations are necessary ingredients when complicated phenomena are to be analysed. We think that the results from the simulations, especially from runs 7–10 indicate that we have actually been successful in simulating the kind of motion giving rise to the $k_h^{-5/3}$-spectra seen in figure 1. Clearly, we have seen a forward energy cascade, just as in three-dimensional turbulence, and the horizontal spectra have a broad $k_h^{-5/3}$-range, just as in classical three-dimensional turbulence. Yet, it is evident that the motion is of a very different kind. Isotropy is a

fundamental feature of classical Kolmogorov turbulence. Mathematically, isotropy means invariance under rotations, i.e. there are no preferred directions. More popularly, we can say that the turbulence looks the same in all directions and is equally distributed over the three velocity components. The kind of motion we have simulated here is radically different. It arises when $F_h \to 0$ and in this limit, the vertical to horizontal length scale ratio l_v/l_h goes to zero, as does the ratio w/u between vertical velocity and horizontal velocity. In this limit, the fluid is stable with respect to generation of classical three-dimensional turbulence, but is unstable with respect to formation of layers. Layers with thickness of the order of $l_v \sim u/N$ are perpetually generated by a basic zigzag type of instability. These layers break down into smaller scales of motions, both in the vertical and the horizontal. Although the vertical range of scales we have been able to simulate is limited, we may interpret the positive energy flux through vertical wavenumbers as evidence of layer formation at successively smaller scales, a process continuing till the layer thickness is of the order of the Ozmidov length scale. As the layers become thinner, they also become sensitive to instabilities which cause them to break up in the horizontal direction. (It is beyond the scope of the present study to investigate the nature of these instabilities, but one obvious candidate is Kelvin–Helmoltz instabilities. It has been shown by Riley & deBruynKops (2003) that such instabilities appear in strongly stratified turbulence at local spots where the Richardson number is small, although the average Richardson number is of order unity.) In this way, a forward cascade is set up.

Despite the fact that $w/u \to 0$, the motion is not two-dimensional, as also pointed out by Billant & Chomaz (2001) and Lindborg (2002). This can be seen from the fact that in the dynamic equations, the nonlinear terms including the vertical velocity are of the same order as the nonlinear terms including the horizontal velocity, i.e.

$$w\frac{\partial u}{\partial z} \sim u\frac{\partial u}{\partial x}, \qquad w\frac{\partial \phi}{\partial z} \sim u\frac{\partial \phi}{\partial x}. \tag{41}$$

A two-dimensional inverse energy cascade can arise when the terms including the vertical velocity are negligible. This is clearly not the case here. Instead, we have seen the case of a cascade which is as different from both the three-dimensional turbulence cascade and the two-dimensional cascade as these two classical cases are different from each other.

Dewan (1979) speculated that the physical mechanism behind the $k_h^{-5/3}$-range is a forward energy cascade, just as in three-dimensional turbulence, but that the cascade is not between 'eddies' which are statistically isotropically distributed in space, as in three-dimensional turbulence, but between 'waves' which have a distinct orientation in the field of gravity. He also suggested that the spectrum is determined by the flux of energy from large to small scales, which is equal to the dissipation ϵ, and a universal constant, corresponding to the Kolmogorov constant of three-dimensional turbulence, but with a different value. In the present study, we have verified that this picture, to a certain extent, is correct. We made the assumption that there are, in fact, two different constants, one associated with the kinetic energy flux according to (35) and one associated with the potential energy flux according to (36). However, as far as the numerical accuracy permitted us to determine these two constants, they were found to take the same value: $C_1 \approx C_2 = 0.51 \pm 0.02$. We leave it to a future study to investigate if there are any theoretical arguments that would permit us to reduce these two constants to a single one. The computed value $C_1 = 0.51$ is not too far from the value 0.67 which was estimated by Lindborg & Cho (2001*a*) from measurements of second- and third-order structure functions using stratospheric aircraft wind data. The $k_h^{-5/3}$-range

of the one-dimensional Nastrom–Gage kinetic energy spectra seen in figure 1 can be fitted to the curve $E_{K_h}(k_h) = 9.1 \times 10^{-4} (\mathrm{m^2\,s^{-3}})^{2/3} k_h^{-5/3}$. With $C_1 = 0.51$, this would give $\epsilon_K = 7.5 \times 10^{-5}\,\mathrm{m^2\,s^{-3}}$, which is very close to the value $\epsilon_K = 6.0 \times 10^{-5}\,\mathrm{m^2\,s^{-3}}$, estimated by Cho & Lindborg (2001) from structure function calculations.

In 1997, Dewan also suggested that the $k_h^{-5/3}$-range in the horizontal spectra seen in figure 1 and the k_v^{-3}-range in the vertical spectra seen in figure 2, originate from the same dynamics. It is true that we have not been able to reproduce a k_v^{-3}-range in the vertical spectra. However, we should not expect it to be easy to reproduce such a spectrum numerically. Carnevale, Briscolini & Orlandi (2001) claim to have reproduced a k^{-3} buoyancy spectrum range in large-eddy simulations of forced stratified turbulence. However, their spectrum should not be interpreted in the light of the hypothesis presented in this paper, since it is not a vertical spectrum, but is computed as an average over all directions. Moreover, it is not a statistically stationary spectrum, but produced just after events of strong wave breaking. To reproduce a vertical k_v^{-3} spectrum according to the present hypothesis, we must resolve a range of vertical scales, r_v, for which $l_O / F_{h_{crit}}^{1/2} < r_v \ll l_v \ll l_h$, while the corresponding condition for reproducing the horizontal $k_h^{-5/3}$ spectrum is to resolve a range of horizontal scales, r_h, for which $l_O / F_{h_{crit}}^{3/2} < r_h \ll l_h$, which is a far less restrictive condition. Let us assume, as was done by Lindborg (2002), that the relation (7) holds, not only for the thickest layers participating in the cascade motion, but also for all thinner layers which are embedded in the thicker layers. If r_v and r_h are the vertical and horizontal length scales of such a layer then we should have

$$r_h \sim \frac{N^3}{\epsilon} r_v^3. \tag{42}$$

This cubic relation means that the thickest layers are the most elongated and the thinnest layers are the least elongated. A variation of r_v by a factor of 10 would imply a corresponding variation of r_h by a factor of 1000. To obtain one decade of a vertical k_v^{-3}-spectrum in a simulation we would therefore have to produce about three decades of a horizontal $k_h^{-5/3}$-spectrum in the same simulation. If $k_{h_{min}}$ and $k_{v_{min}}$ are the smallest horizontal and vertical wavenumbers participating in the cascade, then it is easily argued that $k_{h_{max}} / k_{h_{min}} \sim (F_{h_{crit}} / F_h)^{3/2}$, while $k_{v_{max}} / k_{v_{min}} \sim (F_{h_{crit}} / F_h)^{1/2}$. The reason that we have not been able to reproduce the k_v^{-3}-spectrum is probably that this range is much narrower and does not appear as fast with decreasing F_h as the $k_h^{-5/3}$-range. This is probably also the reason why the vertical k_v^{-3}-spectrum is not as invariably observed as the horizontal $k_h^{-5/3}$-spectrum and that there is still some debate on the exact form of this spectrum. In most studies, the vertical spectra are observed to follow a power law k_v^{-m}, where m is somewhat smaller than 3. Our conjecture is that this is due to a lack of asymptotics in the free atmosphere. The Froude number is on the limit where a clear stationary k_v^{-3}-spectrum appears. Despite the lack of success in simulating the k_v^{-3}-spectrum, there is strong indirect evidence in the present study that it arises from the same dynamics as the $k_h^{-5/3}$-range. Indeed, according to (7) we should look for the vertical one-dimensional spectra corresponding to the horizontal $k_h^{-5/3}$-spectrum, in the range of wavenumbers where we do find the k_v^{-3}-spectrum. This leaves us with little room for alternatives to the hypothesis that these ranges originate from the same dynamics.

There is one important respect in which we want to deviate from the ideas put forward by Dewan and that is his description of the stratified cascade motion as

consisting of a system of linear internal gravity waves which are 'saturated' in the same sense as surface ocean waves are saturated according to the theory of Phillips, (1966). In the ocean wave theory of Phillips, saturation is introduced as a phenomenon opposed to and excluding the phenomenon of a cascade. He writes: 'It appears that the wave interactions are usually incapable of transferring energy from a given wave-number band as rapidly as it is supplied by the wind'. Instead, energy is lost from each wave by the mechanism of breaking which also restores the stability of the wave. According to his eloquent description, energy is fed into each mode by the wind field and sucked out from the same mode in 'intermittent patches of foaming' or 'white horses', i.e. small-scale turbulence. A wave which is maintaining its energy balance in such a process is becoming 'saturated'. In the system of motion we have investigated here, energy is fed into only a few modes, corresponding to the largest wave lengths and all other modes receive their energy from nearby modes in Fourier space and give it away to other nearby modes in a continuous cascade. Energy is sucked out of the system by diffusion in the smallest wave lengths, but there is no gap between these and the other wave lengths in the system. Following Phillips, we find it useful to use 'saturation' to describe a phenomenon which is essentially different from, and excludes, the phenomenon of a cascade. Doing this, there is no doubt that the motion we have investigated here is an example of a cascade motion, rather than a saturated wave motion. If the term 'wave' should be used at all, it is clear that we are not dealing with linear waves. If we were dealing with a system, which to the lowest order could be considered as consisting of linear internal gravity waves, then to the lowest order, we would have perfect equipartition of kinetic and potential energy in each Fourier mode. This would imply that $E_{K_h}(k_h) = E_{P_h}(k_h)$, which is also a consequence of the saturated-cascade theory of Dewan (1997). In our simulations, we instead have $E_{K_h}(k_h) \approx 3E_{P_h}(k_h)$ in the $k_h^{-5/3}$-range. This is far from perfect equipartition.

Indeed, there is an important property of the motion which we have studied here which is wave like, and that is its strong directional dependence, or 'polarization', in the language of wave theory. It appears that this directional dependence is so strong, that it is not only a statistical feature of the system, but a feature of each basic entity of the system. The question is, what term we should use for such an entity? Despite the strong 'polarization', we suggest that the term 'wave' should be avoided, since there is a risk that this will lead to the notion of a linear wave. Instead, we suggest that the more neutral term 'layer' should be used. The most important conclusion to be drawn from the present study is that layer formation is a nonlinear cascade process which is universal for strongly stratified fluids.

There is one important question which is to be given a preliminary answer before we conclude this paper. If the formation of layers and the associated forward cascade process is universal in strongly stratified fluids, why does it make itself apparent at $l_h \approx 500\,\mathrm{km}$ in the free atmosphere and not at the very largest planetary scales? There is only one reasonable answer to this question, and that is that the effect of the rotation of the Earth, which has been neglected in this study, will prevent the forward cascade at larger horizontal scales. The critical value of the Rossby number $Ro = \epsilon^{1/3}/f_o l_h^{2/3}$ ($f_o = 2\Omega \sin\theta$ is the Coriolis parameter. Ω is the rotation rate of the earth and θ is the latitude) over which the strongly stratified cascade can prevail can be estimated from atmospheric data to $Ro_{crit} \approx 0.1$, which is a surprisingly low value, corresponding to a fairly fast rotation. Indeed, in the companion paper (Lindborg 2005) we make a series of simulations with different rates of system rotation and show that $0.09 < Ro_{crit} < 0.14$.

Although layers may form even in rotating fluids, the thickness of the layers will increase with the degree of rotation, which is a well-recognized fact. As an example, we can cite Dritschel, de la Torre Juárez & Ambaum (1999) who write: 'Rotation favors the formation of 'deep' flows having weak variations along the axis of the fluid's rotation . . . , whereas stratification favors the formation of 'shallow' flows having strong variations across stratification surfaces.' As the variation in the vertical becomes smaller with increasing rate of rotation, the nonlinear term including the vertical velocity will become negligible, which means that there will be no horizontal vortex stretching and the forward energy cascade is inhibited, as shown in the theory of quasi-geostrophic turbulence by Charney (1971). The conservation of a second quadratic quantity, potential enstrophy, may lead to a forward enstrophy cascade with an associated k_h^{-3}-spectrum. It is still an open issue whether the narrow k_h^{-3}-range seen in figure 1, can be identified with such a range. This will be investigated in a future study.

On a non-rotating planet, surrounded by a strongly stratified atmosphere, layer formation would totally dominate all fluctuating atmospheric motions superimposed on the mean circulation, from the very largest scales down to the scales where the effect of stratification would become too weak to sustain the stratified cascade. Somewhat counter-intuitively, a strongly stratified atmosphere on a non-rotating planet should therefore be as least as, or even more, turbulent and 'violent' than on a rotating planet.† On a rapidly rotating planet, on the other hand, quasi-geostrophic motions would prevail from the very largest scales down to very small scales where we would see a direct transition to classical three-dimensional turbulence. In the case between these two extremes, such as our own planet, there is a length scale l_h at which there is a transition from a state dominated by rotation with no forward energy cascade to a state dominated by stratification with a forward energy cascade. In fact, $l_h = 500\,\mathrm{km}$ coincides with the standard value which is often given for the Rossby deformation radius, which is 'the scale at which rotation becomes as important as stratification' according to standard textbooks. In the companion paper (Lindborg 2005), we quantitatively demonstrate how the forward energy cascade in a strongly stratified fluid is prevented by system rotation, by presenting another series of box simulations of the Boussinesq equations with different rates of system rotation.

I thank the following persons for fruitful interactions during the development of the present study: Edmond Dewan, Lars Arneborg, Paul Billant, Peter Bartello, Jim Riley, Mike Waite and Tony Burden. Financial support from the Swedish Research Council is gratefully acknowledged.

† It would be interesting to test the strongly stratified cascade hypothesis developed in this paper against data from Venus which is a very slowly rotating planet having a rotation period of 243 days. Having done some preliminary work, we have found nothing in the literature that would contradict that the atmosphere of Venus might be exposed to a very strong energy cascade of the type described in the present paper. Despite its stable stratification, the atmosphere of Venus is full of turbulence (see Izakov 2002 and references therein) and there are several violent dynamic phenomena which are not yet understood, of which the most spectacular is super-rotation. The outer part of the atmosphere is rotating with a period of four terrestial days, i.e. about sixty times faster than the planet. It is generally believed (see Taylor 2002) that the momentum required to sustain this rotation is transferred from the ground by some agent, supposedly some type of wave. Another possible transfer agent would be a layer cascade field extending itself from the very largest planetary scales down to very small scales.

Appendix. The energy growth in $k_\rho = 0$ modes

In three recent numerical studies (Smith & Waleffe 2002; Laval *et al.* 2003; Waite & Bartello 2004) of strongly stratified turbulence it has been observed that there is a weak growth of kinetic energy in modes for which $k_\rho = 0$, or so called 'shear modes'. Smith & Waleffe (2002) interpreted this energy growth as a sign of an inverse energy cascade, which sets in if the Froude number is below a certain critical value. This interpretation is not consistent with our results. Waite & Bartello (2004) were more inclined to attribute the phenomenon to the artificial periodic boundary conditions. Waite & Bartello (2005) also made the interesting observation that the effect seems to disappear in the presence of system rotation. We think that the effect may have multiple causes. We agree with Waite & Bartello (2004) that the periodic boundary conditions are most probably a part of the reason behind the energy growth. It is a reasonable guess that the kind of almost 'crystalline' states seen in the end of the simulations by Smith & Waleffe, with layers filling the whole box, should be more easily obtained in a rectangular box with periodic boundary conditions than in some other geometry with other boundary conditions. The weak forcing we have applied in shear modes, responsible for 1 % of the total energy injection and introducing some phase scrambling into these modes, may be a part of the reason why we have not generally observed the energy growth. On the other hand, in runs 9 and 10, we have shut off this part of the forcing, without observing any growth of total energy.

Although the growth of energy in shear modes may have multiple causes, we think that the main reason behind it is a viscous effect which becomes important when the layer thickness is not sufficiently large as compared to a viscous length scale. If the Froude number is successively decreased without a corresponding decrease of the vertical resolution, then the number of vertical resolution points per layer, $l_v/\Delta z$, will decrease accordingly, and so will the effective Reynolds number based on layer thickness. At some point, the Reynolds number is so low that the layers will stop to break up sufficiently fast to be destroyed at the same rate as they are produced and energy balance cannot be maintained. In Fourier space this will result in a growth of energy in $k_\rho = 0$ modes. This explanation may seem to contradict the finding of Laval *et al.* that the growth in $k_\rho = 0$ modes did not decrease as they increased the Reynolds number. However, the Reynolds number, R_λ, they define is not directly based on a vertical length scale. It is very clear from the vertical spectra in their figure 10, that there is a very strong decrease of the vertical length scale with increasing R_λ. This is also pointed out in their figure capture. It is therefore likely that the layer thickness has, in fact, decreased as compared to the diffusion length scale, as they increased R_λ during the simulation.

If this hypothesis is correct, with Navier–Stokes viscosity, we should see no growth of energy in shear modes if

$$\frac{l_v}{\eta} \sim F_h Re_h^{3/4} \sim F_h^{1/4} Re_v^{3/4} \gg 1, \tag{A 1}$$

where η is the Kolmogorov scale. On the other hand, if this condition is not met, it is possible that we would see something that would be tempting to interpret as an inverse energy cascade, however, which is basically a low-Reynolds-number effect. The layers which are formed in the presence of stratification and stabilized by viscosity will extend themselves indefinitely in the horizontal. According to this interpretation, the growth of energy in shear modes should not only be attributed to the artificial boundary conditions or any other arbitrary feature of the numerical method, but

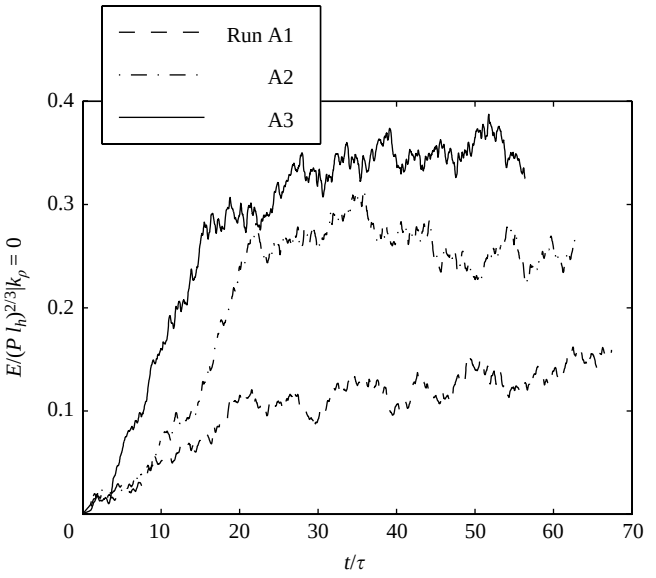

FIGURE 21. Energy growth in shear modes.

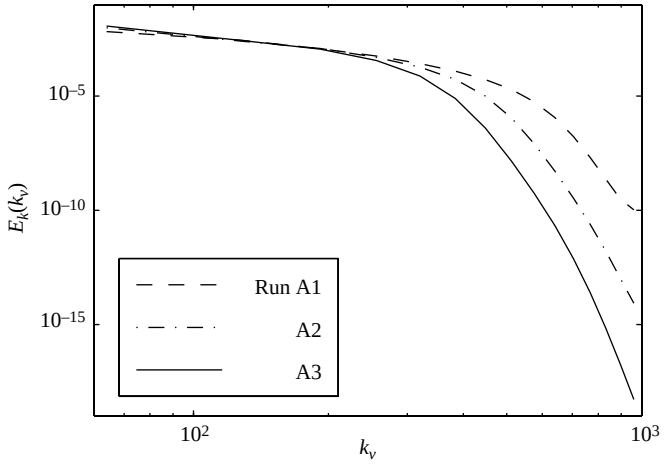

FIGURE 22. Vertical kinetic energy spectra.

can be an effect which has its counterpart in nature, in cases when the condition (43) is not met. Since we do not use Navier–Stokes viscosity in our simulations, it is impossible for us to test this condition quantitatively. However, as pointed out by one of the reviewers, if our hypothesis is correct, we should see an increased growth in shear modes if we increase the vertical diffusion, leaving everything else unchanged. To investigate whether this happens, we have run three more simulations. The parameters are the same as in run 4, except the vertical diffusion coefficients, which are set to $\nu_v = \kappa_v = 3.12 \times 10^{-21}$, 2.57×10^{-20} and 1.32×10^{-19} in the three runs which we label as A1, A2 and A3. In figure 21, the evolution of energy in the shear modes is plotted for the three runs. As can be seen, the growth of energy is strongest in run A3 with the largest vertical diffusion and weakest in run A1 with the smallest vertical diffusion. While the total energy is reaching its stationary value after a few eddy-turnover times,

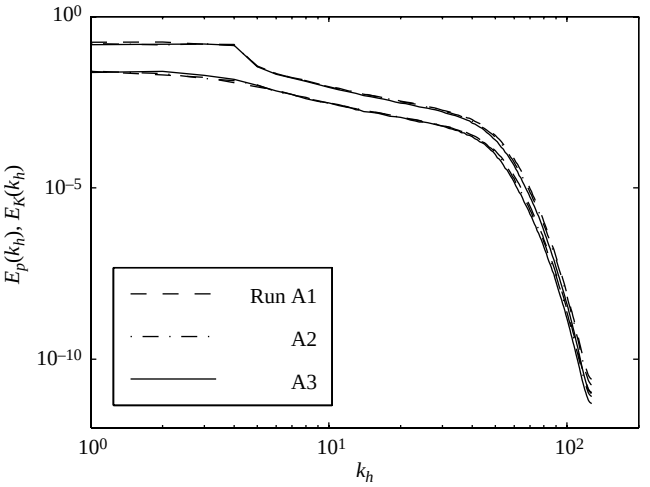

FIGURE 23. Horizontal kinetic and potential energy spectra.

it obviously takes a little longer for the energy content in the shear modes to reach a stationary value. As a matter of fact, there seems to be a weak growth of energy also after $t/\tau = 20$ in run A1 with the smallest vertical diffusion. However, this growth is negligible, since it is smaller than $0.001P$. In fact, all three runs are very close to statistical stationarity from $t/\tau = 20$, and the dynamics in the three runs are very similar to each other. The mean values of ϵ_K and ϵ_P agreed to within three digits between the three runs and the total mean dissipation was calculated to $\epsilon = 1.000$ in all three runs. The mean values of potential energy and the energy content in the vertical velocity component agreed to within two digits. In fact, the only significant differences we saw between the three runs were the difference in the kinetic energy content in the shear modes and the difference in the high wavenumber part of the vertical spectra. In figure 22 we have plotted the vertical kinetic energy spectra, and the difference between the degree of vertical diffusion is clearly reflected in the high wavenumber part. In figure 23, we have plotted the horizontal energy spectra for the three runs. As can be seen, there are no important differences here.

We can draw three conclusions from these results. First, the energy growth in shear modes will decrease with decreased vertical diffusion. In the ideal case of very high Reynolds number, the effect will probably disappear. Secondly, the fact that the energy growth in shear modes varied so much between our three test runs without any significant variation in other quantities, indicates that this growth has little influence on the overall dynamics of our simulations. Thirdly, the fact that the horizontal energy spectra showed no significant change when we varied the vertical diffusion coefficients indicates that our results for the horizontal spectra are robust.

REFERENCES

ALISSE, J.-M. & SIDI, C. 2000 Experimental probability density functions of small-scale fluctuations in the stably stratified atmosphere. *J. Fluid Mech.* **402**, 137–162.

ALVELIUS, K. 1999 Random forcing of three-dimensional homogeneous turbulence. *Phys. Fluids* **11**, 1880–1889.

BILLANT, P. & CHOMAZ, J.-M. 2000*a* Experimental evidence for a new instability of a vertical columnar vortex pair in a strongly stratified fluid. *J. Fluid Mech.* **418**, 167–188.

Billant, P. & Chomaz, J.-M. 2000*b* Three-dimensional stability of a vertical columnar vortex pair in a stratified fluid. *J. Fluid Mech.* **419**, 65–91.

Billant, P. & Chomaz, J. M. 2001 Self-similarity of strongly stratified inviscid flows. *Phys. Fluids* **13**, 1645–1651.

Bolgiano, R. 1959 Turbulence spectra in a stably stratified atmosphere. *J. Geophys. Res.* **64**, 2226–2229.

Carnevale, G. F., Briscolini, M. & Orlandi, P. 2001 Buoyancy- to inertial-range transition in forced stratified turbulence. *J. Fluid Mech.* **427**, 205–239.

Charney, J. G. 1971 Geostrophic turbulence. *J. Atmos. Sci.* **28**, 1087–1095.

Cho, J. Y. N. & Lindborg, E. 2001 horizontal velocity structure functions in the upper troposphere and lower stratosphere 1. Observation. *J. Geophys. Res.* **106**, 10 223–10 232.

Cot, C. 2001 Equatorial mesoscale wind and temperature fluctuations in the lower atmosphere. *J. Geophys. Res.* **106**, D2, 1523–1532.

Dewan, E. M. 1979 Stratospheric spectra resembling turbulence. *Science* **204**, 832–835.

Dewan, E. M. 1997 Saturated-cascade similitude theory of gravity wave spectra. *J. Geophys. Res.* **102**, D25, 29 799–29 817.

Dewan, E. M. & Good, R. E. 1986 Saturation and the 'Universal' spectrum for vertical profiles of horizontal scalar winds in the atmosphere. *J. Geophys. Res.* **91**, 2742–2748.

Dritschel, D. G. & de la Torre Juárez, M. 1996 The instability and breakdown of tall columnar vortices in a quasi-geostrophic fluid. *J. Fluid Mech.* **328**, 129–160.

Dritschel, D. G., de la Torre Juárez, M. & Ambaum, M. H. P. 1999 The three-dimensional vortical nature of atmospheric and oceanic turbulent flows. *Phys. Fluids* **11**, 1512–1520.

Frisch, U. 1995 *Turbulence*. Cambridge University Press.

Gage, K. S. 1979 Evidence for a $k^{-5/3}$ law inertial range in mesoscale two-dimensional turbulence. *J. Atmos. Sci.* **36**, 1950–1954.

Godeferd, F. S. & Cambon, C. 1994 Detailed investigation of energy transfers in homogenous stratified turbulence. *Phys. Fluids* **6**, 2084–2100.

Godeferd, F. S. & Staquet, C. 2003 Statistical modelling and direct numerical simulations of decaying stably stratified turbulence. Part 2. Large-scale and small scale anisotropy. *J. Fluid Mech.* **486**, 115–159.

Herring J. R. & Métais, O. 1989 Numerical experiments in forced stably stratified turbulence. *J. Fluid Mech.* **202**, 97–115.

Izakov, M. N. 2002 Turbulent heat fluxes in the atmosphere of Venus. *Sol. Syst. Res.* **36**, 193–205.

Kaneda, Y., Ishihara, T., Yokokawa, M., Itakura, K. & Uno, A. 2003 Energy dissipation rate and energy spectrum in high resolution direct numerical simulations of turbulence in a periodic box. *Phys. Fluids* **15**, L21–L24.

Kraichnan, R. H. 1970 Inertial-range transfer in two- and three-dimensional turbulence. *J. Fluid Mech.* **47**, 525–535.

Koshyk, J. N. & Hamilton, K. 2001 The horizontal kinetic energy spectrum and spectral budget simulated by a high-resolution troposphere–stratosphere–mesosphere GCM. *J. Atmos. Sci.* **58**, 329–348.

Laval, J.-P. McWilliams, J. C. & Dubrulle, B. 2003 Forced stratified turbulence: succesive transitions with Reynolds number. *Phys. Rev.* E **68**, 036308.

Lilly, D. K. 1983 Stratified turbulence and the mesoscale variability of the atmosphere. *J. Atmos. Sci.* **40**, 749–761.

Lindborg, E. 2002 Strongly stratified turbulence: a special type of motion. *Advances in Turbulence* IX, Proceedings of the Ninth European Turbulence Conference, Southampton.

Lindborg, E. 2005 The effect of rotation on the mesoscale energy cascade in the free atmosphere. *Geophys. Res. Lett.* **32**, L01809.

Lindborg, E. & Cho, J. Y. N. 2000 Determining the cascade of passive scalar variance in the lower stratosphere. *Phys. Rev. Lett.* **26**, 5663–5666.

Lindborg, E. & Cho, J. Y. N. 2001*a* Horizontal velocity structure functions in the upper troposphere and lower stratosphere 2. Theoretical considerations. *J. Geophys. Res.* **106**, 10 233–10 241.

Lindborg, E. & Cho, J. Y. N. 2001*b* Determining the cascade of kinetic energy and scalar variance in the lower stratosphere. *Turbulence and Shear Flow Phenomena*, Proceedings of the Second International Symposium, KTH Stockholm.

Lumley, J. L. 1964 The spectrum of nearly inertial turbulence in a stably stratified fluid. *J. Atmos. Sci.* **21**, 99–102.

Lundbladh, A., Berlin, S., Skote, M. *et al.* 1999 An efficient spectral method for simulation of incompressible flow over a flat plate. *Trita-mek. Tech. Rep.* 1999:11 KTH.

Métais, O., Bartello, P., Garnier, E. *et al.* 1996 Inverse cascade in stably stratified rotating turbulence. *Dy. Atmos. Oceans* **23**, 193–203.

Nastrom, G. D. & Gage, K. S. 1985 A climatology of atmospheric wavenumber spectra of wind and temperature observed by commercial aircraft. *J. Atmos. Sci.* **42**, 950–960.

Nastrom, G. D., Gage, K. S. & Jasperson, W. H. 1984 Kinetic energy spectrum of large-and mesoscale atmospheric processes. *Nature* **310**, 36–38.

Phillips, O. M. 1966 *The Dynamics of the Upper Ocean.* Cambridge University Press.

Riley, J. J. & deBruynKops, S. T. 2003 Dynamics of turbulence strongly influenced by buoyancy. *Phys. Fluids* **15**, 2047–2059.

Skamarock, W. C. 2004 Evaluating mesoscale NWP models using kinetic energy spectra. *Mon. Weather. Rev.* **132**, 3019–3032.

Smith, L. M. & Waleffe, F. 2002 Generation of slow large scales in forced rotating stratified turbulence. *J. Fluid Mech.* **451**, 145–168.

Smith, K. S. 2004 Comments on 'The k^{-3} and $k^{-5/3}$ energy spectrum of atmospheric turbulence: quasigeostrophic two-level model simulation'. *J. Atmos. Sci.* **61**, 937–942.

Taylor, B. I. 1935 Statistical theory of turbulence. *Proc. R. Soc.* A **151**, 421–478.

Taylor, F. W. 2002 Some fundamental questions concerning the circulation of the atmosphere of Venus. *Adv. Space Res.* **29**, 227–231.

Tung, K. K. & Orlando, W. W. 2003 The k^{-3} and $k^{-5/3}$ energy spectrum of atmospheric turbulence: quasigeostrophic two-level simulation. *J. Atmos. Sci.* **60**, 824–835.

Waite, M. L. & Bartello, P. 2004 Stratified turbulence dominated by vortical motion. *J. Fluid Mech.* **517**, 281–308.

Waite, M. L. & Bartello, P. 2005 The transition from geostrophic to stratified turbulence. *J. Fluid Mech.* (submitted).

Vinnichenko, V. K. 1970 The kinetic energy spectrum in the free atmosphere – 1 second to 5 years. *Tellus* **22**, 158–166.